Biomorphodynamics of river banks in vegetated channels with self-formed width

Biomorphodynamics of river banks in vegetated channels with self-formed width

Simone Zen, Paolo Perona

School of Engineering, University of Edinburgh, Scotland, UK

Abstract

Laboratory and field studies investigating the mutual interaction between riparian vegetation dynamics and river morphodynamics have revealed that riparian vegetation may play an important role in the evolution of channel beds and river banks. In order to disentangle this still debated question, field and modeling techniques have helped to explore and better understand the time and spatial scales of such processes. Simple morphodynamic models for river evolution have typically used a constant discharge to describe in-channel processes and basic relationships for river bank dynamics. In order to overcome these limits we propose a longitudinally integrated dynamical model that describes the bank pull - bar push mechanisms in channels with symmetric cross section. Different hydrographs (constant, periodic and stochastic discharge) are applied to investigate channel width and vegetation biomass evolution trajectories and equilibrium values. Results show the interplay of riparian vegetation and water flow in controlling channel width evolution and the trajectories of channel adjustment to flow perturbations. These results also highlight the limit of adopting a constant discharge when describing mutual flow and vegetation processes affecting channel evolution.

Preprint submitted to Advances Water Resources *December 5, 2019*

In addition, under stochastic forcing, the model shows the existence of a range of flood frequencies for which the cooperation between the hydrologic time scales and that characterizing vegetation colonization induces a regular pattern in channel width time variations (coherence resonance). Finally, model application to real case studies confirm the possibility to use the model to interpret long-term river evolutionary trajectories in realistic applications.
Keywords: bio-morphodynamic model, dynamical system, bank deposition, vegetation colonization, channel width temporal adjustments, stochastic water discharge

1. Introduction

The mutual interaction between riparian vegetation and river processes has been found to control the morphological evolution of lateral infinitely erodible channels (Gurnell, 2014). Plants growing on the river banks modify sediment properties driving the width toward which the river tends to adjust (Micheli et al., 2004; Allmendinger et al., 2005). Channel width is the result of the balance between erosional and depositional processes controlling the migration rate of the river banks.

Whether a channel undergoes narrowing, widening, or maintaining a balance between the advancing/retreating rate of the banks, thus retaining an almost constant channel width, depends on how water flow interacts with the sediment budget, river morphology, and the properties of the floodplain, i.e. vegetation coverage and sediments type. The rate at which river banks retreat is associated with fluvial erosion processes and bank failure mechanisms (Darby et al., 2007; Rinaldi et al., 2008).

In vegetated floodplains, plants exert a positive feedback through their roots on the stability of river bank reducing bank failure frequency (Micheli and Kirchner, 2002; Gasser et al., 2019). The strengthening effect of plant roots and the presence of fine sediments provide cohesion to the sediment of the bank, generating a cohesive layer on the top of a non-cohesive one (Pizzuto, 1984), which may affect bank erosion (Thorne, 1990).

Laboratory experiments exploring the interaction between flow, sediments, and vegetation have confirmed field observations that vegetation can control bank erosion, channel width, and river planform evolution (Tal and Paola, 2010; Van Dijk et al., 2013), towards single thread channels (Braudrick et al., 2009). Whilst many field and laboratory studies indicate a positive effect of vegetation on bank stability, other field observations have revealed that in forested margin, trees-toppling associated to fluvial erosion further increases the bank retreat rate (Pizzuto et al., 2010).

The above ground biomass also plays a fundamental role in the dynamics of river banks. During floods, riparian plants interact with overbank flow inducing deposition of fine sediments and aggrading the bar surface, which generates benches that contribute to the accretion of the bank (Erskine et al., 2009). This favours the progressive shifting of the bank margin and induces cross section narrowing (Friedman et al., 1996; Thorne, 1998; Erskine et al., 2012) with the channel possibly adjusting toward a new morphological equilibrium (Eekhout et al., 2014).

Field observations on active branches of meandering rivers confirmed this be a fundamental mechanism in the evolution of natural meander bends (Nanson, 1981; Gurnell and Petts, 2006; Zen et al., 2017). Vegetation en-

croachment growing on bar deposits or dead wood stranded on the point bar, retain sediments, moisture, and nutrients, allowing the creation of a suitable environment for seeds to sprout and grow (Gurnell et al., 2001). Once established, plants consolidate bar sediment through their root systems, thus increasing the resistance of the bar to erosion by flow and generating additional protection for the bank. The reduced channel width then increases the erosion at the cutting bank during the subsequent flood pushing it away (i.e. bar push). The newly-generated wider cross section will allow new sediments to be exposed, and colonized, leading the inner river bank to advance again (i.e. bank pull).

Modeling research has explored the above biomorphodynamic processes to provide insights into their physical controls. Because bank erosion represents a relevant problem for river management this has long received considerable research attention. Numerical models of river bank flow-related dynamics have been proposed to understand how vegetation biomass reinforces river banks (Pollen and Simon, 2005; Langendoen et al., 2009) or how its presence can promote bank failure (Wiel and Darby, 2007). Simple models have included the overall influence of vegetation on bank stability as an increased friction angle or bank strength to explore river planform morphology (Millar, 2000; Eaton et al., 2010). Other modeling effort have included the presence of vegetation on physically-based morphodynamic models for river evolution to investigate how its presence influence river planform (Murray and Paola, 2003; Crosato and Saleh, 2011). Finally, more complex bio-morphodynamic models have coupled riparian vegetation dynamics with river morphodynamics to explore the evolution of river bars (Bertoldi et al., 2014; Caponi and

Siviglia, 2018) and meandering bends (Perucca et al., 2007; Oorschot et al., 2016; Zen et al., 2016).

Although riparian vegetation seems to play a crucial role in controlling river morphodynamics in vegetated river corridors (Camporeale et al., 2013; Gurnell, 2014) there is also evidence that this is not the *sine qua non* condition to establish a stable single thread morphology. Laboratory observations on the erosion of channel banks have shown that fine sediments mixed with coarse non-cohesive sediments provide sediment cohesion, which prevents runaway widening and maintains single thread channel evolution (Parker, 1998; van Dijk et al., 2013). Such results have been further supported by studies conducted on meandering rivers wandering in non-vegetated floodplains such as in modern desert basins (Santos et al., 2019), and on the surface of Mars (Matsubara et al., 2015). These studies have revealed how rivers preserving single thread channels are seen to be devoid of riparian vegetation (Ielpi, 2018). Other experiments focusing on the dynamics of bar push and bar pull provided evidence of the fact that fine sediments deposited on the coarse sediments of a point bar generates morphological structures similar to scroll bars (van de Lageweg et al., 2014). The application of models on the long-term planform evolution of meandering rivers has also proven a long-term control on the erosion rate of meanders banks. As a consequence of their spanning back and forth during their evolution river meanders self-build their floodplain, locally modifying its erodibility properties (Bogoni et al., 2017).

Morphodynamic models for river planform evolution have traditionally adopted the hypothesis of i) a constant channel width, and ii) constant dis-

charge. In particular, such models take advantage of the fact that the relevant erosion processes occur at a different temporal scale of the in-channel morphodynamics (Ikeda et al., 1981; Seminara, 2006). Modeling efforts within the past years have introduced a local imbalance between the advance and retreat rates of the opposite banks to explore channel width temporal variations (Parker et al., 2011; Eke et al., 2014; Lopez Dubon and Lanzoni, 2018; Monegaglia et al., 2019). In this type of models the two opposites banks can either erode or deposit proportionally to the excess of shear stress (longitudinal velocity) experienced at the bank toe through a erosion (E_e) and deposition (E_d) coefficient. The proposed simplified closures are of the type $\xi_E = E_e\,(\tau_s - \tau_c)$ when $\tau_s > \tau_c$ and $\xi_D = E_d\,(\tau_s - \tau_c)$ when $\tau_s \leq \tau_c$; where τ_s and τ_c is the shear stress and its critical value for sediment movement respectively. Although, the authors have referred to E_d as the coefficient accounting for vegetation dynamics and their interaction with alluvial sediments, the aforementioned relationship for bank evolution can also be applied for other physical controls responsible for the advancing of the floodplain margin (e.g. sediment mixture).

The local expansion and contraction of the channel width in time can not be explored by models based on a constant, formative, discharge (Pizzuto, 1994). Flow variability in time is fundamental to the erosional and depositional processes in both bare and vegetated channels. In the latter, periods of low discharge allow vegetation to colonise and grow. Weather during a flood vegetation decays or survives, stabilizing the alluvial sediments of the bank, depends on how the hydrological and biological processes interact at relevant/different time scales (Perona et al., 2012).

Although the influence of flow stochasticity and river morphology on the vegetation dynamics has largely been investigated (e.g. Camporeale and Ridolfi, 2006; Doulatyari et al., 2014; Vesipa et al., 2017; Bertagni et al., 2018), its feedback on the river morphology, and on the interaction between vegetation and river processes, in particular, is poorly understood. Perucca et al. (2007) used the model proposed by Camporeale and Ridolfi (2006) to link the timescales of the vegetation growing on the floodplain with the lateral migration of evolving meandering channels. To account for the frequency with which the channel is found to be morphodynamically active, Eke et al. (2014) introduced a flood intermittent factor while keeping the water discharge constant. Zen et al. (2016) proposed a hybrid biomorphodynamic lumped model for bank accretion to quantify the influence of river flow variability on the in-channel bio-morphodynamics controlling the bar push - bank pull mechanism in evolving meander bends.

Recently, Davidson and Eaton (2018) have tried to overcome the constant-discharge approach by including randomness in investigating river channel morphology evolution. In their lumped model a series of random-yearly floods erode the channel banks, while a random coefficient, accounting for plant colonisation controls channel narrowing. The model allowed the authors to obtain channel cross sections whereby the generated geometry depended both on the water discharge and the history contingency.

In this work we propose a simple lumped model for river biomorphodynamics where the two banks can either erode or advance toward the center of the channel as a result of the mutual interaction (push-pull mechanism) between near-bank fluvial processes and vegetation dynamics growing on the

banks. The model is used to investigate i) the role of flow discharge (external driver of the system) in selecting the channel width to which the channel tends to adjust, and ii) how the interaction between vegetation dynamics, sediment erosion and water discharge temporal scale influences channel width time and spatial scales. To these aims different types of hydrographs including deterministic and stochastic external forces are adopted.

The work is structured as follows. In Section 2 the model is presented along with the assumptions adopted and used to investigate the dynamical properties of the system. In Section 3, results obtained for the different water discharge that includes constant, periodic and stochastic flow are presented and discussed. Finally, Section 4 presents the application of the proposed model to three real cases and Section 5 is the conclusion section of the paper.

2. Methods

We propose a model that mimics the key mechanisms for which plants growing onto the river bar stabilise the sediments and contribute to channel narrowing until geomorphic relevant floods erode the bank and uproot riparian vegetation. Temporal variation in channel width are thus related to vegetation dynamics, which in turn is modulated by the channel flow rate. Although trees toppling can destabilise the bank increasing the rate of bank retreat, in the model only the positive feedback of vegetation that increases channel bank stability is accounted for. Hereinafter, an asterisk will indicate dimensional quantities. Figure 1 presents a schematic of the lumped model proposed.

2.1. Bio-morphodynamic Model and related Assumptions

We model an erodible straight channel characterised by homogeneous non-cohesive sediments, with a representative size diameter of d_s^*, and a bed slope, S. To keep the model simple, a series of hypotheses have been introduced. We consider a wide channel, such that the hydraulic radius can be approximated with the water depth; the channel cross section is rectangular and symmetrical, thus the banks either advance or retreat of the same quantity. Moreover, the model is lumped in the sense that it is integrated along the streamwise direction following the work of Cantelli et al. (2007), and Tealdi et al. (2011).

Other considerations on the temporal scales of the processes are worth some further explanation/clarification. In-channel morphodynamic processes occur at a time scales faster than that characterising river banks migration, and colonisation and stabilisation by vegetation dynamics. Because of this, the sediment flux between the channel and floodplain region can be considered negligible, and bank advance and retreat can be modeled as continuous processes (Howard, 1992; Lanzoni and Seminara, 2006). Under these hypotheses, bank retreat is linearly related to the excess of near-bank shear stress. We assume that the material eroded at the bank is immediately transported out of the section without modifying the channel bed. In the model, we account for the shear stress value through the dimensionless Shields number and the relationship for river bank erosion (Partheniades, 1965) reads

$$\frac{dw^*}{dt^*} = E^* \left(\tau_s - \tau_{form}\right)^{\alpha}, \tag{1}$$

where w^* is the channel width, t^* is the time, τ_s is the longitudinal Shields number, E^* is a erodibility coefficient accounting for bank material properties

and α is a positive constant assumed to take the value 1 (Darby and Rinaldi, 2007). The value τ_{form} represents the critical value of the Shields number for bank erosion, such that if the Shields number exceeds this value the channel will widen.

Based on the assumption that rivers adjust themselves such to maintain a bankfull Shields number (Parker et al., 1998), Eke et al. (2014) showed that the equilibrium channel characteristics can be estimated once channel slope, grain size, friction coefficient and bankfull discharge are known. Thus, by following Eke et al. (2014), the formative Shields number in the erosion relationship (1) for the channel bank τ_{form} has been set equals to the equilibrium value of near-bank Shields number associated to the bankfull flow discharge, Q_0^* and width w_0^*, in a non vegetated channel. This implies that, if there are no changes in water flow or channel width and vegetation does not grow, then channel banks are neither eroded nor aggraded. Thus, in the model, the bankfull condition represents the reference state of the river.

Previous works modeled river banks advancements by adopting a closure relationship similar to equation (1) for bank erosion. In this work, bank advancement is directly related to vegetation dynamics, which has direct influence on sediment processes. By growing during the low flow, vegetation consolidates the exposed sediments of the fluvial bar, and the channel narrows according to the relationship

$$\frac{dw^*}{dt^*} = -r_1^* \rho^*(t^*) w^*(t^*), \tag{2}$$

where r_1^* is a coefficient accounting for the rate of colonization of the vegetation, ρ^* is the vegetation biomass. The negative sign is introduced since we consider channel widening as positive. The narrowing term is linearly

related to the channel width to account for the fact that when the channel is wide the reduced water depth promotes vegetation growth, thus channel narrowing.

In order for vegetation to populate the bank during low flow an aggrading surface connecting the river bed with the floodplain is required, e.g the typical transverse profile of fluvial bars. Lumped models studying channel bank erosion have adopted a trapezoidal section and expressed the shear stress experienced at the inclined sidewalls as a fraction of the channel bed shear stress (Cantelli et al., 2007; Tealdi et al., 2011). To keep the problem at the minimum level of complexity, we consider the bank vertical whereby the vegetation is able to withstand bank erosion and thus a rectangular cross-section (Figure 1). In addition, the overbank flow is neglected assuming that all the hydrograph peaks can be contained within the main channel.

When the channel is eroding the banks, and thus widening the section, we assume a rectangular cross-section without bed forms, which is consistent with the analysis of Zen et al. (2014). Building up from the work of Tubino (1991), (Zen et al., 2014) showed that during high flow the generation of bars is hampered but that the widening process promotes channel bed instability leading to the deposition of bars. Channel widening promotes both channel bed instability and vegetation colonisation by lowering the water depth. Therefore, we assume that when the discharge is not high enough for bank erosion, a bar generated during a previous formative event is present and its exposed sediments can be colonised by vegetation.

By taking advantage of the different time scales between river hydrodynamics and bank dynamics, we can also interpret changes in water flow rate

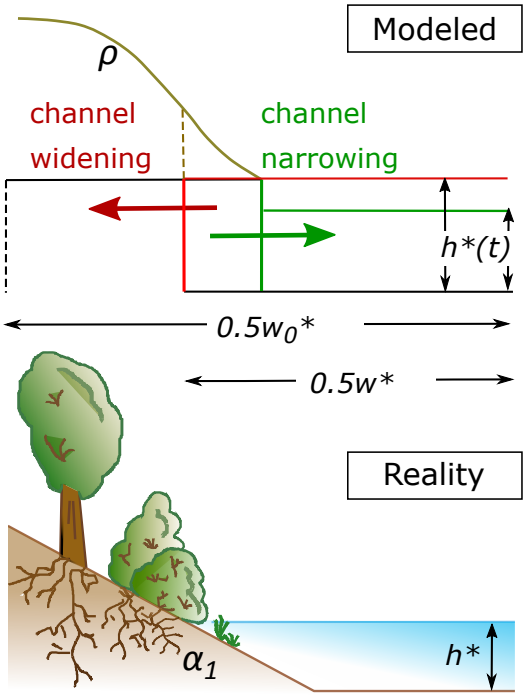

Figure 1: Sketch of the modeling framework. w_0^* is the initial channel width, w^* is the time dependent channel width, h^* is the water depth associated to the water discharge Q^* flowing into the channel of width w^*, slope S and sediment size d_s^*, ρ is the continuous distribution of vegetation biomass, and α_1 accounts for the sediment cohesion induced by plant roots (equation (4)). The red and green arrow indicate channel widening due to erosion and channel narrowing due to plant colonisation respectively.

as a sequence of instantaneous uniform flows and assume the river slope to be constant in time. At the reach scale, the river channel slope changes on larger temporal scales than those associated with channel width adjustments. Therefore, we assume the channel responds to changes in water discharge by modifying its width rather than aggrading-degrading the bed (Howard, 1980). Under the hypothesis of normal flow and shallow flow approximation, the shear stress is equal to the product of the fluid density, gravity acceleration, bed slope and water depth, and the Shields number reads

$$\tau_s(t^*) = \frac{h^*(t^*)S}{\Delta\ d_s^*} = \frac{1}{\Delta d_s^*}\left(\frac{SQ^*}{C^* w^*}\right)^{(2/3)}, \tag{3}$$

where Δ is the relative submerged weight of the sediment (1.65 for quartz material), h^* is the water depth, Q^* is the related water flow discharge, and C^* denotes the Chezy friction coefficient.

In order to account for the increased resistance to sediment erosion due to the presence of plant roots (Yang et al., 2018), the critical value for the Shields number is defined as follows (Zen et al., 2016):

$$\tau_{form} = \tau_{form,0}(1 + \sigma_1 \rho^*), \tag{4}$$

where $\sigma_1 \leq 1$ is a positive coefficient linking below-ground biomass (plant roots) with the above-ground biomass ρ, and $\tau_{form,0}$ is the threshold value for the near-bank Shields number in absence of vegetation. Vegetation growth dynamics follows a logistic curve, whereas vegetation decays because of channel bank erosion when the longitudinal shear stress falls above its formative

threshold. The biological dynamics is described by the following equations

$$\frac{d\rho^*(t^*)}{dt^*} = \frac{r^*}{t_v^*}\rho^*(t^*)\big[\beta^* - \rho^*(t^*)\big] \tag{5}$$

$$\frac{d\rho^*(t^*)}{dt^*} = -\rho^*(t^*)\tau_\Delta(t^*)E^*\frac{1}{w^*(t)} \qquad \tau_\Delta > 0, \tag{6}$$

where β^* represents the vegetation carrying capacity (maximum biomass reachable under optimal conditions), r^* is the curve growth rate that determines the time scale t_v^* representing the time vegetation takes to grow from the 5% to 95% of the carrying capacity, and $\tau_\Delta = (\tau_s(t^*) - \tau_{form}(t^*))$. In equation (6) vegetation decay is inversely related to channel width to account for the increase in water depth associated with channel narrowing that promotes vegetation removal, and the subsequent channel widening. The temporal evolution of the two states variables of the system, namely river channel width w^*, and vegetation biomass ρ^*, is thus described by the following system of non-linear, coupled, ordinary differential equations

$$\frac{dw^*(t^*)}{dt^*} = E^*\tau_\Delta(t)\Theta(\tau_\Delta) - r_1^*\rho^*(t^*)w^*(t^*) \tag{7}$$

$$\frac{d\rho^*(t^*)}{dt^*} = \frac{r^*}{t_v^*}\rho^*(t^*)\big[\beta^* - \rho^*(t^*)\big] - \rho^*(t^*)\tau_\Delta(t)\Theta(\tau_\Delta)E^*\frac{1}{w^*(t)}; \tag{8}$$

where the parameter $\Theta(\tau_\Delta)$ is the Heaviside step function which sets to null the positive term of equation (7) when the Shields number falls below its formative value. Hence, channels narrow because of colonising vegetation on the bank. While growing, vegetation increases sediments resistance to erosion thus allowing the bank to advance (second term of the right-hand-side of equation (7)). This reduces the channel section, which in turn induces vegetation removal, bank erosion and channel widening during subsequent floods (Figure 1).

It is worth clarifying that there is a high degree of uncertainty in the choice of the values of the constants accounting for the vegetation colonisation rate, r_1, and the increased resistance to sediment erosion provided by plant roots, σ_1. This is mainly due to the absence in the literature of physically based relationships that would allow such parameters to be estimated on the base of measurable characteristics of the river channel. Because of this uncertainty, in the following analysis we will explore a range of values to quantify their influence on the overall channel width and vegetation biomass.

Dimensionless equations

We first rewrite the model in dimensionless form. To this aim, let us introduce the following dimensionless quantities:

$$t^* = tt_0^* = tt_v^*, \qquad w^* = w_0^* w, \qquad Q^* = Q_0^* Q, \qquad E^* = E\frac{w_0^*}{t_0^*}, \tag{9}$$

$$\rho^* = \rho\beta^*, \qquad r^* = \frac{r}{\beta^*}, \qquad r_1^* = r_1 r_2^* = r_1\frac{r}{t_0^*\beta^*},$$

having denoted with t_0^* a typical temporal scale of the process, i.e. the time t_v^*, and $r_2^* = r^*/t_0^*$. The Shields number can be therefore expressed as:

$$\tau_s = \frac{1}{\Delta d_s^*}\left(\frac{SQ_0^*}{C^* w_0^*}\right)^{(2/3)}\left[\frac{Q(t)}{w(t)}\right]^{(2/3)} = \tau_{s,0}\left[\frac{Q(t)}{w(t)}\right]^{(2/3)}; \tag{10}$$

where $\tau_{s,0}$ is the Shields number associated to the initial, bankfull, channel configuration. The model (7, 8) can now be rewritten as:

$$\frac{dw(t)}{dt} = E\tau_\Delta(t)\Theta(\tau_\Delta) - \gamma\rho(t)w(t) \tag{11}$$

$$\frac{d\rho(t)}{dt} = r\rho(t)\Big[1-\rho(t)\Big] - \rho(t)\tau_\Delta(t)E\frac{1}{w}. \tag{12}$$

The parameter $\gamma = r_1 r$ accounts for the rate of colonisation of vegetation having set r constant and equal to 5.88, which allows the vegetation to grow

from 5% to 95% of its maximum in a time equals to t_v^* ($t = 1$ in dimensionless quantities).

2.2. River hydrology

To define the influence of hydrologic stochasticity on the control of vegetated channel width we will explore the response of the system to either deterministic or stochastic hydrologic forcing. The use of a characteristic discharge is usually adopted in analytical models for river morphodynamics. The value is normally chosen so as to generate the same equilibrium geometry produced by the long-term hydrograph. In this analysis, the equilibrium bankfull geometry in the absence of vegetation corresponds to the bankfull discharge, $Q_0 = 1$.

We will also explore the response of the system forced with a periodic flow oscillation of the type

$$Q(t) = Q_0 + 0.5sin(f2\pi t); \tag{13}$$

where f is the signal frequency that can be interpreted as mean hydrograph fluctuations. It is worth mentioning that a periodic pattern in the hydrological signal can be observed in natural catchments characterised by a nivo-pluvial regime.

For the stochastic analysis, we will use a synthetic hydrologic signal characterized by a series of instantaneous flood events occurring randomly with random magnitude, hereinafter denoted to as 'jumps', followed by an exponential deterministic decay. Under this assumption the stochastic hydrological signal is described by the Langevin equation

$$\frac{dQ}{dt} = -\frac{Q}{\theta} + \sum_{i=1}^{\infty} p_i(t)\delta\left(t - t_i\right); \tag{14}$$

where θ indicates the rate of discharge decay after the positive jump p_i occurred, and $\delta(\cdot)$ is the Dirac delta distribution. We also assume both jumps intensity, p_i, and their interarrival time to be distributed according to exponential functions whose parameters are, respectively, the jumps average, α, and their average daily frequency, λ. In this case and under the assumption that jumps occur as a independent and identically distributed uncorrelated process, equation (14) describes the dynamics of the so-called Compound Poisson Process - CPP (Doulatyari et al., 2014). The probability distribution of the discharge values, p_Q, generated from these hypothesis is a gamma function with mean μ_Q and variance σ_Q^2 can be estimated analytically (Botter et al., 2007; Ridolfi et al., 2011). For the sake of completeness let us introduce the coefficient of variation C_v, that indicates the magnitude of variation around the series mean value, as $C_v = \sigma_Q^2/\mu_Q$.

In lowland alluvial rivers the rising limb of the hydrograph is characterized by a mild slope. Yet, in such catchments the falling limb last longer compared to that typical of mountains streams, which increases the correlation, θ of the hydrological signal. Thus, the stochastic process generates correlated rising limbs as a sequence of jumps and exponential decays.

3. Results and Discussion

3.1. Linear stability analysis

We study the isoclines and the nullclines (i.e. $dw/dt = 0$, $d\rho/dt = 0$) of the system to determine the nature of the equilibrium point and how it is influenced by the system parameters. When the system is forced with deterministic hydrologycal action the equilibrium values for the two state

variables, w and ρ, can easily be assessed analytically by equating their temporal derivatives to zero. The first equation, (11), provides the equilibrium value for the vegetation biomass

$$\rho_{eq} = \frac{1}{1 + r_1} \tag{15}$$

which can be substituted into the second equation, (12), to derive the equilibrium value for channel width. However, the influence of channel width on the Shields number introduces a strong non linearity in the equation that does not allow to obtain an explicit relationship for the equilibrium channel width $w_{eq}(Q, E, \sigma_1, \tau_{s,0}, \gamma)$. Yet, such a value can be computed once assigned the characteristic for channel geometry, hydrology and vegetation type, by solving the following equation

$$\xi_2 w_{eq}^{2.5} - \xi_1 w_{eq} = \xi_0 Q, \tag{16}$$

where the coefficients ξ_i, $i = \{0, 1, 2\}$ read:

$$\xi_2 = 1, \qquad \xi_1 = \left(E\tau_{s,0} \frac{1 + r_1 + \sigma_1}{\gamma} \right)^{3/2}, \qquad \xi_0 = \left(E\tau_{s,0} \frac{(1 + r_1)}{\gamma} \right)^{3/2}. \tag{17}$$

Computing the equilibrium values is further complicated by the dependency of the Shields formative value on vegetation. The influence of riparian vegetation on sediment erosion through equation (1) and (4), does not allow us to impose $\tau_\Delta > 0$ to obtain an analytical solution for the equilibrium of the system, preventing a stability analysis to be performed. To overcome this issue we introduce a new continuous function, $\widetilde{\tau_\Delta}$, which is able to provide an analytical approximation for the Heaviside step function originally adopted. The excess of Shields number, τ_Δ, is therefore interpreted as a transcritical

bifurcation (Strogatz, 2018) of a function switching its stable condition between zero, when the Shields number falls below its critical value, and the excess of Shields number itself otherwise. The equation describing the transcritical bifurcation is solved coupled with the equations for channel width and vegetation biomass dynamics, and the new complete system now reads:

$$\begin{aligned}
\frac{dw(t)}{dt} &= E\widetilde{\tau_\Delta}(t) - \gamma\rho(t)w(t) \\
\frac{d\rho(t)}{dt} &= r\rho(t))\Big[1-\rho(t)\Big] - \rho(t)\widetilde{\tau_\Delta}(t)E\frac{1}{w} \\
\frac{d\widetilde{\tau_\Delta}}{dt} &= \left(\tau_\Delta\widetilde{\tau_\Delta}(t) - \widetilde{\tau_\Delta}(t)^2 + \xi\right)\frac{1}{t_\Delta},
\end{aligned} \tag{18}$$

where t_Δ is a temporal scale indicating the rapidity with which the approximation function $\widetilde{\tau}_\Delta$ tends to the solution obtained by adopting the Heaviside function and ξ is a small value (assumed equals to 0.01) that is added to avoid the approximation function to stick to zero. In the following section we will explore the influence of the channel bank erodibilty, E, river hydrology Q, and vegetation characteristics r_1 and σ_1 on the two state variables of the system, namely w and ρ.

The new system of ODE equations (18) allows us now to compute the equilibrium condition for which the temporal derivative are set equal to zero and study its stability. To do this we linearise the system around the equilibrium point $\{w_{eq}, \rho_{eq}, \widetilde{\tau}_{\Delta,eq}\}$ and investigate its eigenvalues. Because one of the three eigenvalues associated to the system refers to the approximation function, only the two eingenvalues λ_1, λ_2 associated to the physical state variables of the system w and ρ will be considered. Figure 2a presents the dependency of the equilibrium values for the channel width from water discharge, Q, and the coefficient σ_1 accounts for sediment strengthening by

plants root. The value presented by the vegetation biomass at the equilibrium is dictated only by the colonisation coefficient r_1, as also noted in equation (15) (Figure 2b). For the sake of brevity the linearised system is reported in Appendix A. The system shows two equilibrium points, one where bank erosion processes balance that of bank colonisation and another one where the unvegetated channel would reach its equilibrium width when the Shields number equals its threshold value for bank erosion ($\tau_\Delta = 0$).

Figure 2d shows that when the value of the vegetation colonisation rate, r_1, is close to zero, the eigenvalues are different negative real numbers, while for $r_1 \geq 0.2$ the two eigenvalues are complex conjugates with the real part invariably negative. Since the real component of the eigenvalues is invariably negative the equilibrium point is an attractive point. This means that bank advancing, induced by vegetation dynamics, and erosion adjust their rate in time until an equilibrium channel width is reached. If the sediment supply is assumed constant, the way the two bank processes cooperate is directly controlled by the vegetation type and the hydrology of the channel. Therefore, in the following, we will explore different river hydrology and different type of vegetation, i.e distinct value of the colonisation parameter r_1 and the constant σ_1 accounting for the increased resistance to sediment erosion associated with plant roots.

In absence of vegetation colonisation ($r_1 \leq 0.2$), or presence of sparse vegetation coverage, the equilibrium point of the system (w_{eq}, ρ_{eq}) behaves as a stable node directly attracting all the trajectories on the phases plane (Kaplan and Glass, 1995). Therefore, when vegetation type presents a low colonisation rate, vegetation biomass increases, reducing the channel width

monotonically, or vice versa, until the equilibrium width is reached. When the eigenvalues are complex conjugates, i.e. $r_1 > 0.2$, the equilibrium point of the system is a stable focus (Kaplan and Glass, 1995) and the fluvial system behaves in a different way. The system state variables present an exponentially decaying oscillation at the rate $e^{\lambda_i t}$ (since the eigenvalues λ_i are negative) which organise all the trajectories lying on the phase plane in a spiral path around the equilibrium point. Therefore, the higher the absolute value of the real component of the eigenvalues, the faster the system reaches the equilibrium condition. Figure 2d shows how the stable focus of the system become rapidly attractive when $r_1 > 0.2$.

When the channel is fed with a variable discharge, the increase in water flow induces channel widening via bank erosion. The widened cross section allows the vegetation to colonise the sediments and grow, advancing the bank and narrowing the channel. This promotes bank erosion that widens the channel removing vegetation biomass, and the cycle restart. However, with every cycle, the survived vegetation will reduce the amount the bank retreats, diminishing also the space available for vegetation to grow, thus the amount the bank advances. When reported in the phase plan the values of the state variable of the system organise on a spiral path. The phase plane presents a more simple path in the case the channel is fed with a constant discharge. Here, vegetation encroachment at the bank narrows the channel section increasing the shear stress, thus promoting bank erosion and biomass removal. As a consequence the channel widens until the equilibrium width value is reached.

Because channel bank accretion and erosion are mutually related, when

the colonisation rate r_1 increases these two bank processes keep pace with each other, maintaining the equilibrium channel width. Yet, a rapid vegetation-related channel narrowing induces strong erosion at the bank leading to an overall reduced vegetation biomass at the equilibrium (Figure 2b). Conversely, the parameter σ_1, accounting for the increased resistance to sediment erosion, modifies the equilibrium channel width without affecting the equilibrium value associated to the vegetation biomass. In this case, the absolute value of the complex and real component of the eigenvalues, respectively increases and decreases linearly with the constant σ_1. Therefore, increasing in plant root strength will augment the attractive force of the equilibrium point while extending the time required to reach the equilibrium by introducing bigger oscillations of the parameters. By hampering bank erosion, plant roots bring an unbalance between the bank processes that promotes the development of narrow channels. Such influence on channel geometry becomes stronger for higher water flow (Figure 2a). Despite the discharge value influencing the equilibrium channel width, it marginally affects the dynamical property of the system with the equilibrium point that remains a stable focus and it is reached at almost the same rate for discharge values bigger than the reference value $Q = 1$, i.e. the real component of the eigenvalues shows very small variations in Figure 2c.

3.2. Deterministic behavior: Constant discharge

We first explore the case of three non vegetated channels fed with a constant discharge equal to the bankfull discharge, $Q = 1$, and different initial channel width (Figure 3a dashed lines). Since the threshold Shields number for bank erosion has been set as equal to the Shields number associated to

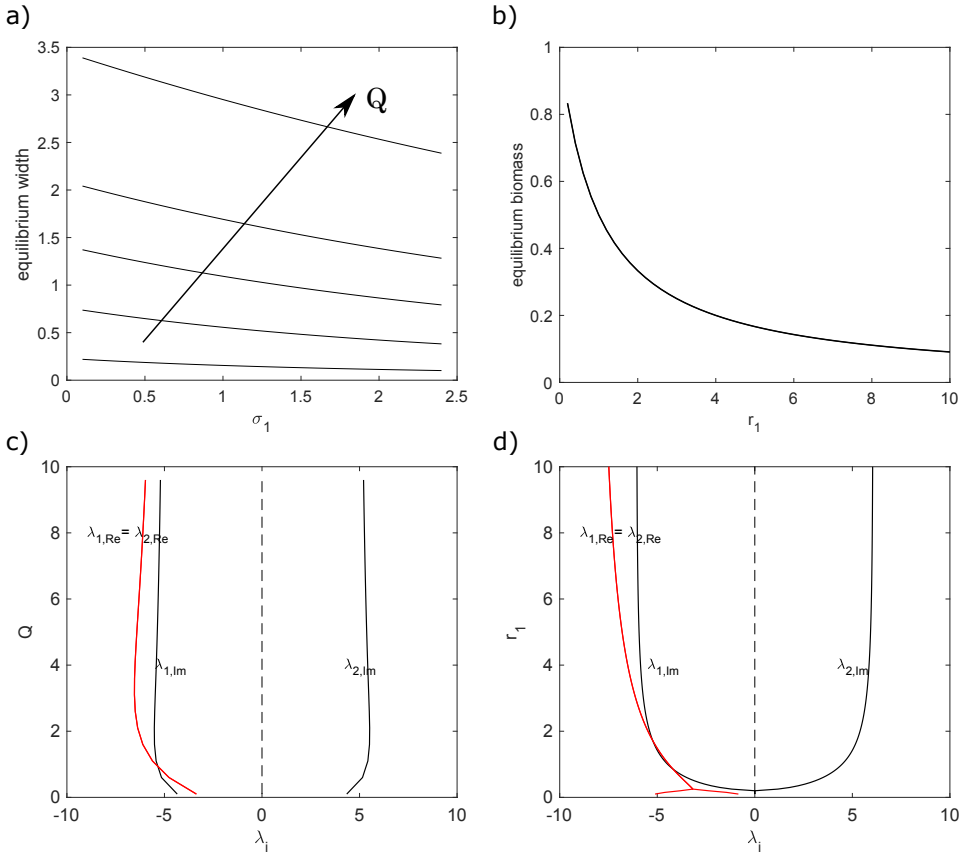

Figure 2: The upper panels show the equilibrium state for the a) channel width against the coefficient σ_1 accounting for the role played by plants root and water discharge, Q; and b) the vegetation biomass for different rate of colonisation, r_1. The lower panels show the eigenvalues for the system (18) associated with the variables w and ρ for different values of c) water discharge Q and d) colonisation rate r_1. When not specified $r_1 = 2$ and Q =1 - $E = 100$, $\sigma_1 = 0.2$.

bankfull conditions, i.e. $w(t=0)=1$ and $Q(t=0)=1$, a channel presenting unitary width maintains its geometry with time. A wider channel, e.g. $w(t=0)=2$, because of the water depth and near bank shear stress will favour deposition at the bank and thus section contraction. However, as the Shields number falls below its threshold value for bank erosion, the channel will neither erode nor deposit thus maintaining the initial channel width. On the other hand, a narrower channel, $w(t=0)=0.5$, due to the higher flow velocity becomes erosional, hence widening its section. This progressively diminishes bank erosion until the system reaches its actual bankfull width and the Shields number equals its threshold value. Conversely, a vegetated channel adjusts to a new equilibrium condition by either eroding or depositing, regardless of its initial geometry (Figure 3a). Indeed, the presence of vegetation activates the narrowing term $dw/dt<0$ in equation (11) which is proportional to the rate of colonization r_1. Figure 3a (green continuous line) shows that for both the bankfull-reference and wider channel, $w(t=0)=1$ and $w(t=0)=2$, respectively, vegetation growth promotes channel narrowing. On the other hand, the narrower channel, $w(t=0)=0.5$, initially increases its width until the channel is wide enough to allow bank advances to reduce the channel width and adjust it to a stable value.

Figure 3b and c show, respectively, how the colonisation rate r_1 and the constant σ_1 influence these processes by modifying their temporal scales and the overall equilibrium condition of the channel. In particular, when the colonisation process is rapid vegetation growth it is not able to keep pace with the rate of bank advance that rapidly increases the shear stress inducing bank erosion, thus vegetation removal. The faster the channel narrows the

lower is the amount of vegetation biomass on the bank, as well as the time needed to reach the equilibrium. Because no changes are introduced on the property of the bank and the shear stress is inversely related to the channel width, therefore the amount that the channel narrows is proportional to that which it widens. Therefore, for $r_1 \geq 1$ the channel tends to recover the same equilibrium width, but it presents lower values of vegetation biomass. On the other hand, changes in the root influence on sediment erosion, i.e. σ_1, determine different equilibrium width without affecting the equilibrium vegetation biomass Figure 3c. In this case the constant accounting for an increased resistance to sediment erosion exerts two effects: i) promotes bank advance and vegetation growth by protecting the bank, ii) reduce channel widening. This does not modify the overall vegetation biomass, but it reduces channel width and increases the rate at which the banks shift. Therefore, the stronger the influence on bank erosion exerted by plant roots the narrower the channel. Such a result is in agreement with field observations on vegetated evolving channels (Allmendinger et al., 2005). Overall, the colonisation rate and the roots strength control the equilibrium vegetation biomass and the equilibrium channel width respectively, and the related time scales. In Figure 3b and c the black line indicates the trajectory associated with $r_1 = 2$ and $\sigma_1 = 0.2$.

From the mathematical point of view, the behaviour of the system in Figure 3b is explained with the conversion of the equilibrium from a stable node to a stable focus and with the increased attraction of this latter, i.e. smaller temporal scales for high r_1 values already discussed in the analysis of the eigenvalues. Moreover, the overshooting that characterises the curves

of Figure 3b is associated with the complex component of the eigenvalues of the system and therefore it is observed only for value of r_1 greater than 0.2 (see Figure 2d). A similar behaviour is observed when the protection to erosion exerts by the plant root increases as reported in Figure 3c. However, in this case, the real component of the eigenvalues decreases, whilst the complex component increases. The complex component is still responsible for the amplitude of the overshooting that progressively increases while the reduced variation of the real component leaves the time required to reach the equilibrium almost unchanged.

Figure 4a and c present the trajectories of the system for different initial values of channel width and vegetation biomass. The blue and green isolines refers to the value of $\frac{dw}{dt}$ and $\frac{d\rho}{dt}$, respectively. The point where the two zero-isolines meet each other is the equilibrium point (black dot). Wide and equilibrium channels always undergo a narrowing process, $\frac{dw}{dt} < 0$, associated with an increase of vegetation biomass, $\frac{d\rho}{dt} > 0$, until a maximum value after which channel width changes slightly while the biomass decreases abruptly. The different trajectories reported on the phase plan of Figure 4a and c show how the initial conditions control the attractiveness of the equilibrium point, with narrower channels, i.e. $w(t = 0) < 1$, reaching the equilibrium condition faster than the wider ones, i.e. $w(t = 0) \geq 1$.

We now explore the influence of the erodibility coefficient, E, on the dynamics (Figure 4a and c). By increasing bank erodibility the equilibrium channel width, also increases without influencing vegetation biomass. Simulation runs conducted for different water discharge ranging from 0.5 to 2 with $r_1 = 2$ reveal a similar behaviour with the river system adjusting to

larger sections for large discharges without modifying the vegetation biomass (red circle in Figure 4b); such that the higher the discharge the wider the equilibrium channel. The equilibrium value for vegetation biomass is indeed controlled by the parameter r_1 that accounts for the ratio at which channel banks advance reducing the channel width. Figure 4b and d show that the influence of the parameter ratio r_1 on the equilibrium value of the channel width is low for $Q <= 1$ and it becomes even lower when bank erodibility increases (almost vertical lines in Figure 4d). The temporal trajectories reported in the phases plan also provide a visualization of the system flow and how it is attracted by the equilibrium point that behaves as a stable focus.

Overall, in channels fed with a constant discharge the presence of vegetation leads to an equilibrium cross section narrower than that estimated by adopting the bankfull discharge. Indeed to recover the bankfull geometry (i.e dimensionless channel width = 1) the vegetated channel should be fed with a constant discharge higher than its bankfull value, with the increased amount set proportional to the ratio r_1. In other words, if the sediment cohesion induced by plant roots is neglected the model should be fed with a water discharge lower than the bankfull value to obtain realistic estimates of the channel width. This result agrees with the findings of Bolla Pittaluga et al. (2014) and Lanzoni et al. (2015) who applied a one-dimensional morphodynamic model to the Magra River (Italy) and Po River (italy), respectively, to explore the role of the formative discharge.

3.3. Deterministic behavior: Periodic discharge

The response of the system undergoing periodical fluctuations of the water discharge around its bankfull value $Q = 1$ shows a behaviour consistent

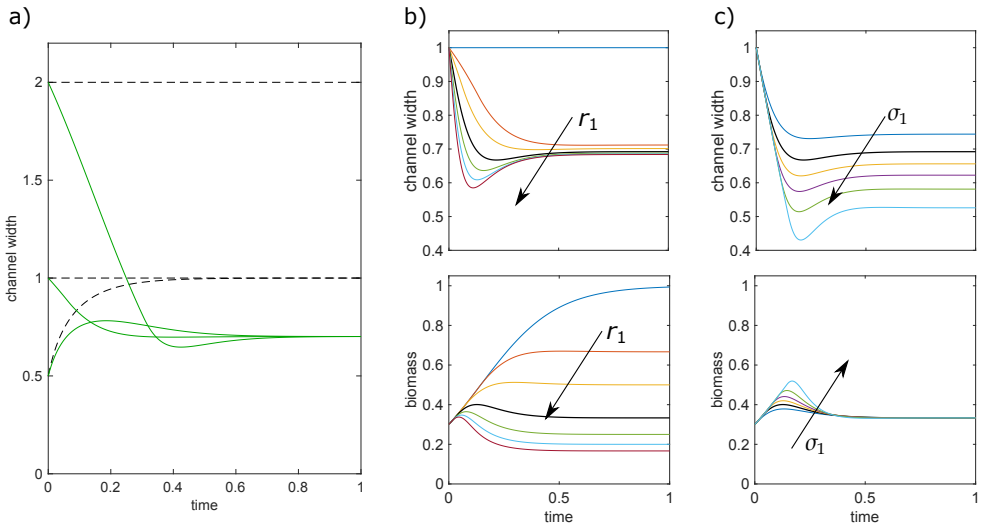

Figure 3: Evolutionary trajectories. a) Comparison between evolutionary trajectories for a non vegetated channel (dashed black line) and a vegetated channel (continuous green line) for different initial values of dimensionless channel width, $w = 0.5,\ 1.0,\ 2.0$, $w = 1$ indicates the bankfull channel width. b) and c) show how the parameter r_1 and $\sigma 1$ influence the same trajectory reported in a) for a vegetated channel initially showing a bankfull cross-section ($w = 1$) and the related biomass ρ - $r_1 = 0{:}5$, $\sigma 1 = 0{:}1$. Other relevant parameters are $E = 100$, $\sigma_1 = 0.2$, $r_1 = 2$ in a), $Q = 1$.

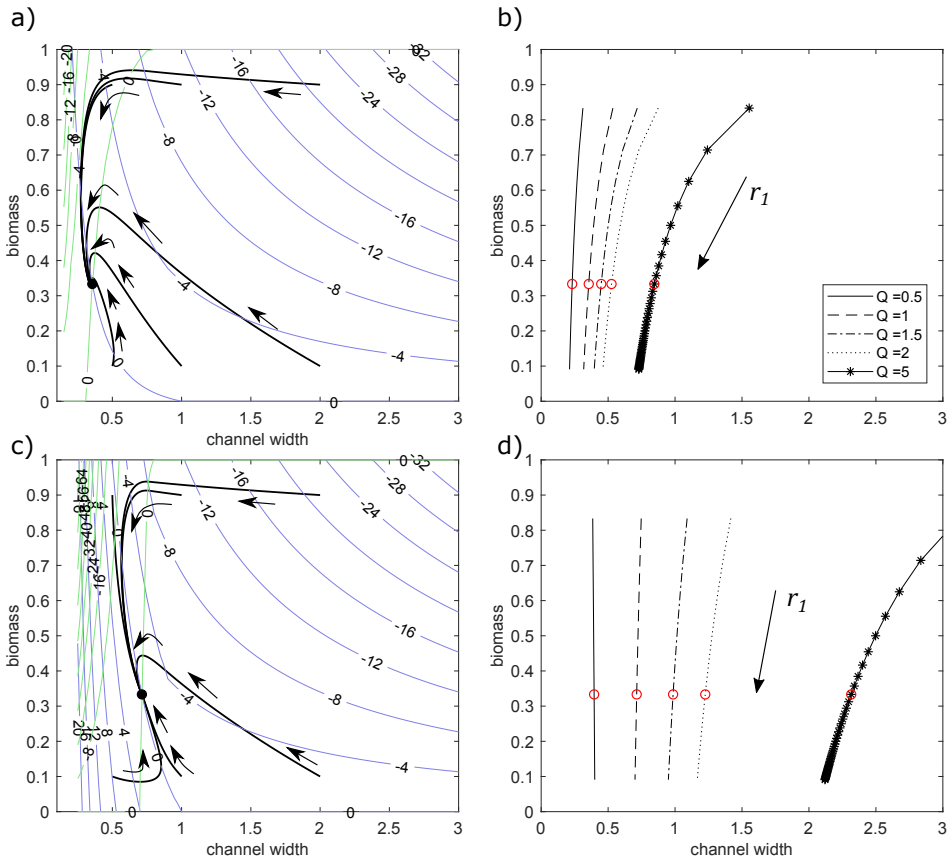

Figure 4: Panels a) and c) phases plane for the system (18) for different initial conditions of vegetation biomass 0.1, 0.9 and channel width 0.5, 1.0, 2.0, and values of erodibility coefficient a) $E = 10$, c) $E = 100$. The blue and green lines represent the 'isolines', which are the locus of points where the time derivative $dw/dt = 0$ and $d\rho/dt = 0$, respectively. Panels b) and d) report the equilibrium point of the system for different values of the dimensionless water discharge $Q = 0.5{:}5$, respectively for b) $E = 10$, and d) $E = 100$. When not specified the relevant parameters for the simulation are $r_1 = 2$ and $Q = 1$. The red circle on panels b) and d) indicates the equilibrium point of the system associated to $r_1 = 2$.

with that observed for the case of constant discharge. The comparison of two deterministic trajectories, respectively associated with a constant and periodical discharge, shows that after a transitory phase the system reaches a steady phase in which it oscillates around an equilibrium state at the same frequency of the hydrologic forcing (Figure 5). The system subject to a periodic discharge undergoes narrowing, then the increased shear stress promotes bank erosion widening the channel. As a consequence the lower depth allows vegetation to colonise the sediment of the bank and narrow down the section. As a result, the two signals of channel width and vegetated biomass oscillate with the same frequency but with opposite phases. This behaviour is controlled by the inertia of the system and the interaction between the bank erosion and colonisation temporal scales.

According to equation (13), the frequency of the hydrologic signal indicates the number of complete cycles of flow increases and decreases within a characteristic vegetation time t_v. Because the hydrologic time scales are directly associated with the vegetation timescales, when the signal frequency is low the limited channel widening is associated with an initial increase in water flow rate promoting vegetation growth. As a consequence, the channel undergoes narrowing allowing vegetation to grow further and resulting in a net increase in vegetation biomass. At this point, because of the new over-narrow section, any increase in water flow will remove vegetation biomass via bank erosion. Figure 5 shows that the amplitude of such temporal variation for both channel width and vegetation biomass is inversely related to the signal frequency. There is however an initial phase, which last almost half of the typical vegetation time t_v, where the state variables of the system present a

trend regardless the frequency characterising the hydrologic forcing. At this stage, the channel width limits the erosional power of the flow, generating a suitable environment for the vegetation to grow. This unbalance between bank advance and retreat results in a negative trend for the channel width and a net increase for vegetation biomass. The channel keeps narrowing until a width of around 0.8 when the erosional processes keep pace with vegetation dynamics and the system oscillates around its equilibrium configuration.

It is worth noting that a higher frequency of the hydrologic signal narrows the evolutionary trajectory to that experienced by the channel when fed with a constant bankfull discharge (dashed line in Figure 5). However, the reduced period of time for which the discharge is higher than the bankfull value promotes channel widening. As a result, the system oscillates around a channel width larger than that to which the bankfull discharge would have set the channel. This is particularly evident for the simulations with frequency $f = 5$ (Figure 5). The amount of time for which the water flow is above or below the average is the same regardless of the number of time the average value is crossed and the fast oscillation does not allow changes in the system that slightly oscillate around the equilibrium condition. This result highlights the limit of using deterministic hydrograph as input for river morphodynamic models.

3.4. Stochastic behavior

While interpreting the response of the system subject to a deterministic forcing is quite straightforward, this may not be the case for stochastic forcing. We start with studying the evolution of the system to a sequence of CCP flood events. Figure 6 shows that in channels where bank colonisation

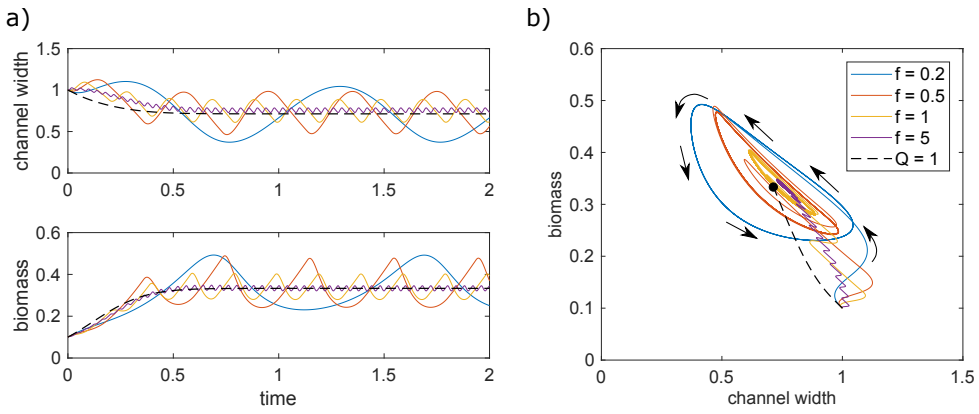

Figure 5: Response of the system to a periodic discharge for different frequencies with which the discharge value oscillates around the formative dimensionless discharge Q_o - $Q(t) = Q_o + 0.5sin(f2\pi t)$ with frequencies f ranging from 0.2 to 5. Panels a) shows the temporal trajectories for both channel width and vegetation biomass; b) the same trajectories presented in a) are reported on the phase plane channel width - biomass.

is hampered by environmental conditions, $r_1 = 0$, the channel keeps its width constant until a flood event able to erode channel banks occurs. In this case vegetation growing on the channel banks is removed. In vegetated channels characterised by vegetation encroachments on the banks, $r_1 > 0$, during low/non formative flow vegetation colonises the banks and grows, reducing the river channel width with a rate that is proportional to r_1 (increasing trajectory slope in Figure 6b). During the subsequent formative flood the reduced channel cross-section increases the near-bank shear stress promoting channel bank erosion and thus vegetation removal. Therefore, flood effects on river channel morphology are not related only to floods magnitude but also to the geometry presented by the channel when a flood occurs. As a consequence initially non-formative floods can generate high bank erosion in

channels that undergoes narrowing because of the mutual interaction between riparian vegetation and river morphodynamics. (Figure 6b).

Model runs performed by forcing the system with a Poissonian stochastic discharge of the type described in equation (14) reveal that the system rapidly looses the configuration set by the initial condition and starts oscillating, randomly, around a steady state configuration. Monte Carlo simulations (only fifty of them are reported in Figure 7 for clarity) allow for extracting the average channel width and vegetation biomass (black solid line in Figure 7) and to obtain the average evolutionary trajectories of the system as well as its equilibrium point. Figure 7 also shows the histogram of the channel width and vegetation biomass values. Interestingly the average evolutionary trajectory, differ from those obtained by forcing the system with constant discharges: equal to the average-CPP discharge (dashed black line in Figure 7) and the bankfull formative discharge, $Q = 1$ (dashed white line in Figure 7), respectively. However, the trajectory associated to $Q = 1$ is quite close to the average trajectory, especially in its final part, showing an equilibrium width slightly larger than the average one. The equilibrium values for the trajectory associated with $Q = 1$ and the average trajectory are, respectively, (0.69, 0.33) and (0.61, 0.35). Nevertheless, this even small difference is due to a change in the system dynamics. By adopting a constant bankfull discharge, the water depth is kept, on average, at higher values than those present in the channel during the low flow periods generated by the stochastic hydrology. This hampers the colonisation process that advances the channel banks and promotes bank erosion, generating a wider channel.

It is instructive to compute the probability distribution of the equilib-

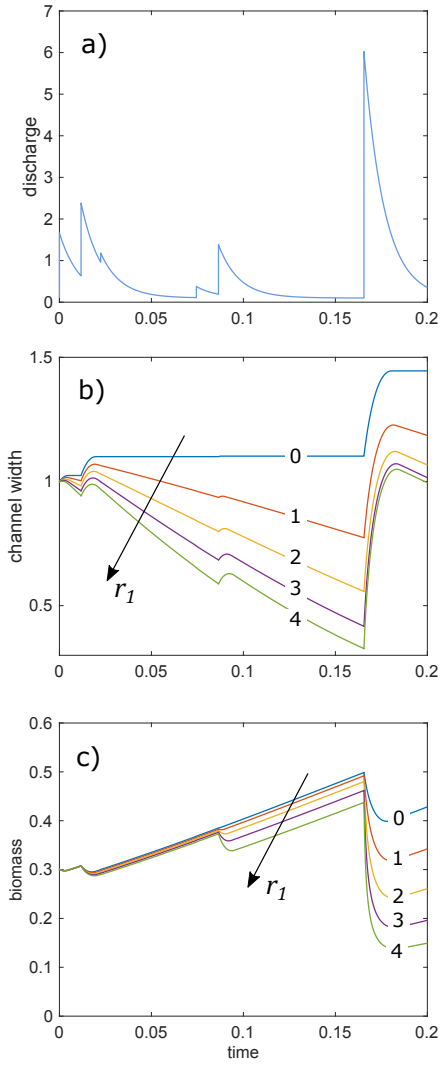

Figure 6: Response of the system to the stochastic hydrograph reported in panel a) for different values of the colonization parameter r_1 ranging from 0 to 4; b) channel width and c) vegetation biomass. Other relevant parameters are: $\mu_Q = 0.6\ m^3/s$, $\tau = 2\ day$, $\lambda = 0.02\ day^{-1}$, $E = 200$, and Initial Conditions $w = 0.1$, $\rho = 0.3$.

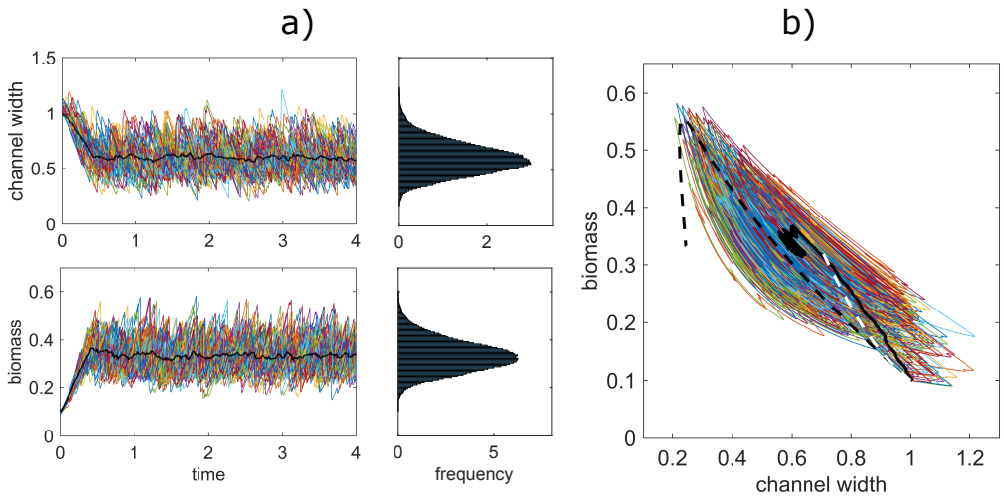

Figure 7: Response of the system to a stochastic hydrologic forcing described by a poissonian process. a) series of 50 distinct stochastic trajectories both for the channel width and the vegetation biomass, with relative histogram. The black continuous line represents the average value for all the 50 realizations at each time. b) the phases plan associated to the trajectories in a). The solid black line represents the average values obtained from the stochastic-runs, while the black and white dashed lines represent the deterministic behaviour of the system fed with a constant discharge equal to μ_Q and 1, respectively. Other relevant parameters: $E = 100$; $\tau = 10$ day; $\lambda = 0.05\ day^{-1}$; $\mu_Q = 0.3\ m^3/s$; $r_1 = 2$; $\sigma_1 = 0.2$.

rium channel width, p_w. The latter is readily obtained from the probability distribution of the water discharge following a classic derived distribution procedure, once the discharge is expressed as a function of the channel width by rearranging the equation (16). The analytical expression for the probability density function of the equilibrium channel width (expressed in equation 16) associated with the distribution of the water discharge reads

$$p_w = \frac{e^{-\frac{\phi}{\alpha}} \alpha^{-\lambda\tau} \left(-\xi_1 - 2.5 w^{1.5} \xi_2\right) \phi^{\lambda\tau - 1}}{\Gamma[\lambda\tau] \xi_0} \tag{19}$$

with $\phi = -(w\xi_1 + w^{2.5}\xi_2)\xi_0^{-1}$ and $\Gamma[\cdot]$ the complete Gamma function (Abramowitz and Stegun, 1965). Notice that this pdf is only attained in the limit of a process always at equilibrium, which is not the case where all dynamics have comparable time scales. Equation (19) does not allow the statistics of the distribution to be computed analytically. Therefore, both the average and standard deviations of the distribution have been estimated numerically.

Figure 8 shows the dependency of the pdf of channel width at the steady state from different parameters of the system, including the average frequency with which floods occur,λ, the colonisation rate, $r1$, and the constant accounting for plant roots σ_1. By increasing the average frequency, λ, the coefficient of variation, C_v, decreases since the discharge mean, μ_Q, linearly increases faster than the variance of the signal, σ_Q^2 - Figure 8a. As a consequence, high floods frequencies induce, on average, wider channels with a distribution presenting larger variance, σ_w^2, compared to that associated to a river characterised by sporadic floods, i.e. low λ values (Figure 8b).

As already observed in the deterministic part of the analysis, the colonisation rate does not affect channel width which is controlled by the strength of plant roots. Different rates of colonisation do not change the average channel

width and have little influence on the overall probability distribution (Figure 8c). Conversely, the channel adjusts to lower average channel width and presents a more peaked and narrow distribution when plant roots are efficient in trapping and retain the bank sediments, i.e. high value of the constant σ_1, in accordance with field observations (Allmendinger et al., 2005) (Figure 8d). We finally explore the role of the channel bank erodibility, E that shows, as expected, an opposite behaviour compared to that of plant roots. Low channel bank erodibility determines more peaked distribution, i.e. lower variance, and lower mean values, when compared with the case of river with highly erodible channel banks. While the variance increases as the erodibility of the channel banks increases, increasing E above 200 slightly modifies the average channel width. As for the periodical case presented above, changes in the average frequency λ with which floods occur (for a given value of τ) control the amplitude of the oscillations of the signal for channel width and biomass. However, a more interesting and less trivial behaviour emerges when the system is forced with a stochastic signal. With this purpose we performed a Fourier analysis of channel width temporal variations away from the transitions due to the influence of initial conditions, paying attention to have a signal that extends at least around 5 times the characteristic time scale of the biomorphodynamic process investigated (t_v). Variations in channel width were analysed on the frequency domain by computing the Power Spectrum. The structure of the signal emerging from the frequency analysis was visualized through a fitting curve computed as the Fourier series of the first eight frequencies given by $w_{Fourier} = a_0 + \Sigma_{i=1}^{8} [a_i sin(\omega_i t) + b_i cos(\omega_i t)]$, where a_0 is the average value around which the channel width oscillates at the steady

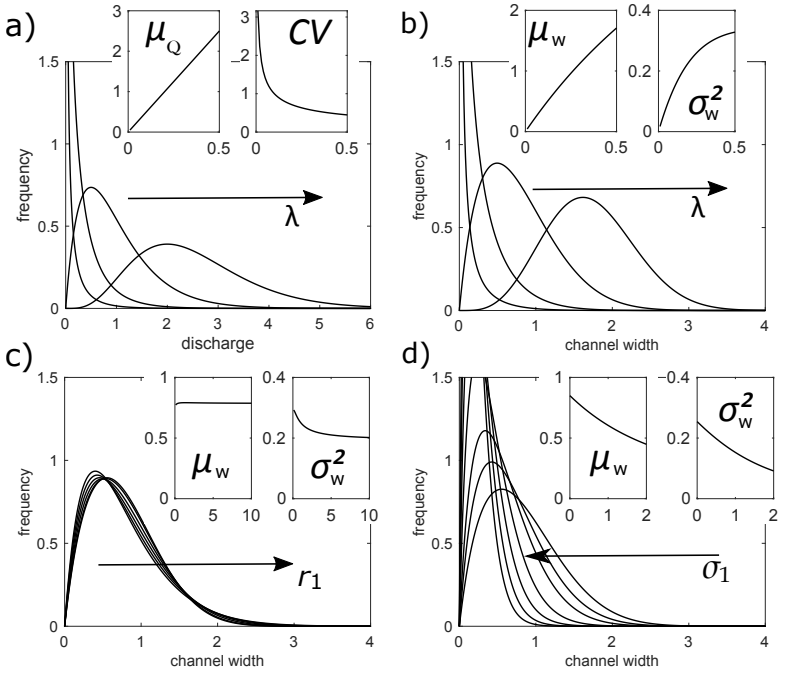

Figure 8: Behaviour of the probability density distribution for the equilibrium channel width, p_w, of a vegetated channel with erodible banks and forced with a CCP characterised by a distribution p_Q. The two upper panels show the dependency of both a) p_Q and b) p_w from the average frequency λ with which the floods occur. Panel c) and d) show, respectively, the dependency of p_w on the colonisation rate of the vegetation, $r1$ and the increased resistance to sediment erosion due to plant roots, σ_1. The close ups present the average value, μ_x and variance, σ_x^2 associated with the distribution p_x. Other relevant parameters: $E = 100$; $\tau = 10$ day; $\mu_Q = 0.5\ m^3/s$; and when not modified $\lambda = 0.2\ day^{-1}$; $r_1 = 2$; $\sigma_1 = 0.2$.

state. Finally, we estimate the autocorrelation function of the signal to interpret any changes in correlation, i.e. memory of the process, associated with the mutual interaction between vegetation dynamics and river processes.

Results show that when the average frequency λ is big (low value of variation coefficient C_v) the forcing signal is weak and channel width oscillates without a clear pattern (Figure 9a), whereas for low frequency values (high value of variation coefficient C_v) the hydrograph presents sporadic almost uncorrelated peaks that generate a narrower channel nevertheless width oscillations do not present a regular organization (Figure 9c). However, there exists a range of intermediate frequencies for which the system seems to recover a more regular (i.e. coherent) variation of the channel width (Figure 9b). This appears more clearly if we consider the signal in the frequency domain and analyse its power spectrum (right column Figure 9). In this new domain the intermediate frequency (Figure 9b) shows a spectrum picked around $\omega = 7$ while high frequencies present a quite flat spectrum (Figure 9a) and the very low frequencies present a spectrum that tends to become flat again since several frequencies show high power. Therefore, only for intermediate λ the system selects a dominant frequency and the response signal to a random noise organizes according to a more regular oscillatory pattern. The Fourier expansion of the signal, for the first eight modes, (red curve in the central panels of Figure 9) visualizes the main oscillating structure for the channel width temporal trajectory.

This process for which noise induces a coherent response in time is known as coherence resonance and it is generated from the interaction of the noise with an intrinsic time scale of the deterministic component of the dynamics

system (Ridolfi et al., 2011). In this case the temporal scale of bank erosion (or vegetation removing), t_b, associated with the Poisson process needs to be compared with that of the deterministic vegetation growth, t_0. When floods occur with low frequency (i.e. t=$t_b >> t_0$) the channel principally narrows with sporadic, random, channel bank erosion that increases channel width. Conversely, when the interval time between two consecutive floods is low (i.e. $t_b << t_0$) the vegetation keeps being removed via bank erosion and the channel undergoes predominantly widening with only random narrowing processes that reduce the section. This sporadic occurrence of channel widening or narrowing with random intensities prevent the formation of a regular pattern. However, when floods occur with an intermediate frequency, under the condition $t_b << t_0$, the vegetation-related channel narrowing counteracts bank erosion and the response of the system shows a quasi-oscillatory behavior.

Simulation runs conducted for different r_1 for a frequency below (0.01) and above (0.03) the intermediate frequency $\lambda = 0.02$ reveal that the colonisation rate itself is not able to reorganize the response of the system in a regular structure (no significant difference in the power spectrum of the signal). However, the colonisation rate does influence the autocorrelation of the signal with an abrupt decrease of the temporal integral scale, i.e. representative time for which the process loose its memory (autocorrelation becomes null), as soon as the colonisation parameter r_1 becomes different from zero. The time integral scale value decreases until a value of r_1 around 4 after which higher values of the colonisation rate do not affect the autocorrelation of the signal. Overall, the control on the channel width exerted by the

colonisation ratio is relevant only for low values of the parameter r_1 (say $<$ 2). This is also supported by the analysis of the eigenvalues that showed how the complex component of the eigenvalues is kept almost constant for value of r_1 larger than 2.

4. Model applications

We applied the model to three study cases: the vegetated flume from the work of Tal and Paola (2010), the restoration project of the Lunterse Beek stream (Eekhout et al., 2014), and that of the River Thur, Switzerland. The three cases were chosen because they represent three single thread reaches whereby changes in channel width can be related to vegetation dynamics. Since the initial configuration of the channel in the laboratory experiments of Tal and Paola (2010) was a braided network, the model has been applied only to the second phase of Run A where a stable single thread channel was formed. Data from the field and laboratory were used to define the initial channel characteristics while the parameter of the model were adjusted to fit the measured valued for channel width in time. The values are reported in Table 1.

Results from model applications to the cases of the run A from Tal and Paola (2010) and the Lunterse Beek stream are shown in Figure 10. For the application to the flume run, the model shows good agreement with the observed evolutionary trend of the single thread reach formed in the flume. The channel progressively narrows due to a net increase in vegetation biomass, until it oscillates around an equilibrium channel width. In the first 4 floods the modeled channel width quantitatively agreed with the wet

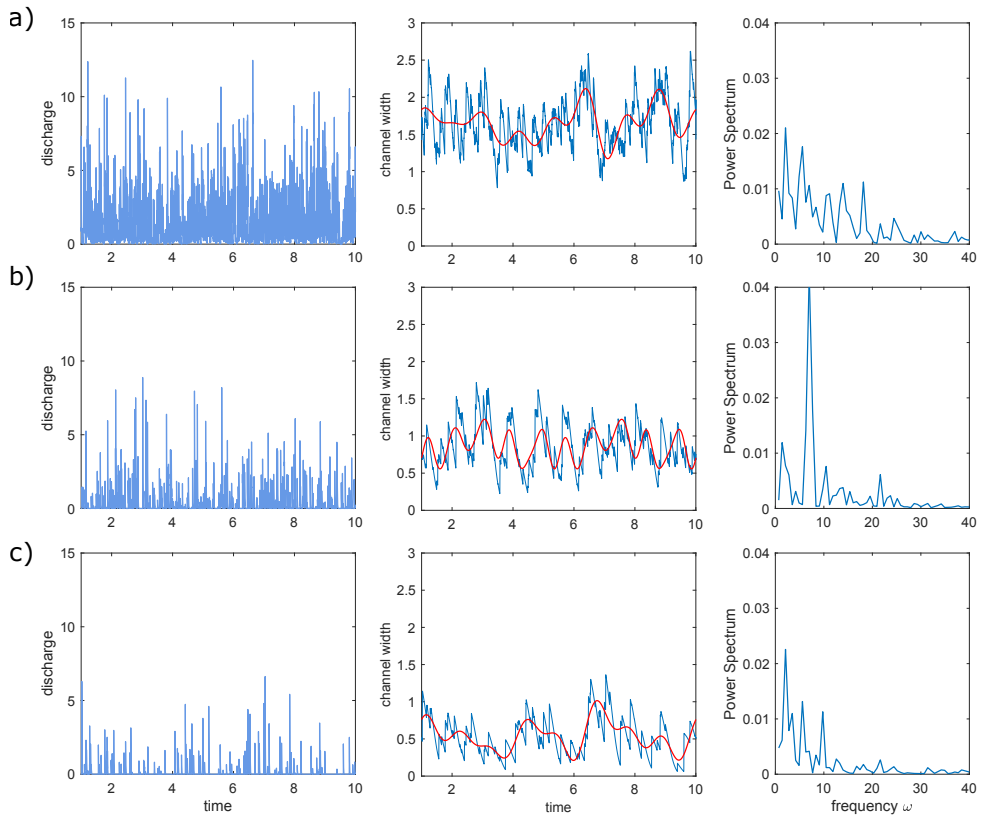

Figure 9: Behaviour of the system subject to a stochastic hydrograph with $\tau = 10\ day$, $\mu_Q = 1.5\ m^3/s$ and $\lambda =$ a) 0.08, b) 0.02, and c) 0.008 day^{-1}. On the left column is reported the stochastic hydrograph, on the central and right columns are presented, respectively, the channel width variations and width signal spectrum associated to the hydrograph on the left. The red continuous line superimposed to the channel width signal on the central panels is the Fourier expansion of the signal computed using the first eight frequencies ω reported on the spectrum panel. Other relevant parameters: $E = 200$; $r_1 = 2$; $\sigma_1 = 0.2$.

width measured during the experiment, while for the second part of the experiment run the model generates larger channel width variation than those measured in the flume (Figure 10a). For the case of the Lunterse Beek stream, the model results are compared with both the channel condition documented by photographs from different dates (Eekhout et al., 2014) and the measurements of channel width (Vargas-Luna et al., 2016). After an initial increasing in channel width associated to occurrence of floods around 100 days from the start of the observation period, the channel underwent narrowing. The subsequent period of low flow allowed the vegetation to grow, restricting the channel cross section until other floods occurred around day 400 widening the channel. However, the increase in water flow discharge was not enough to entirely remove the vegetation that after 500 days could grow narrowing the channel again. Both channel width and vegetation dynamics are well described by the model (Figure 10b). Differently from the case of the flume experiment, in this case the whole predicted evolutionary trajectory shows a good quantitative agreement with the field measurements and field observations, i.e. historical images.

Finally we study a 1.5 km section of the Thur River, Switzerland, that was restored in 2002 to promote the formation of fluvial bars and increase the riparian environment biodiversity. To this aim, river managers and engineers, removed bank protection allowing the river to adjust its channel width that was previously set to 55 m. The active channel width has been estimated from the sequence of aerial images covering a period from 2002 to 2018 (Figure 11 by taking an average of the position of the banks (red lines in the pictures in Figure 11) and neglecting the local increase in channel width due to the

meandering of the channel. The channel width was accounted as the portion of bare channel bed that could have been reworked during a flood.

Model results show that the first floods occurring after the restoration of the channel at the end of year 2002 widen the channel by setting its average channel width to a value almost twice the initial one, i.e. 100 m. In the following three years, the channel narrows to a width of around 90 m, with a flood occurring at the end of the summer 2005 that sets back the channel banks recovering a width of 100 m. This event slightly influences vegetation dynamics and vegetation biomass keeps growing during the following years narrowing the channel. Low magnitude floods generate marginal variations in channel width and vegetation biomass until the end of the summer 2013. Here the channel experiences the biggest flood and bank erosion increases the channel width to 112 m, by reducing the vegetation biomass slightly above 0.6. In the following years, the absence of significant floods allows the vegetation to grow and the channel width recovers to a value of around 80 m. The comparison of model results with the images collected from different dates shows a quantitative agreement for the channel width. In addition, the model catches the temporal dynamics of vegetation biomass. From the images it is possible to observe a low presence of vegetation at the end of 2005, and vegetation encroachment on the exposed bar in September 2008 that grew extending the vegetated portion of bar as observed in the picture from 2009. Starting from 2013 vegetation progressively grows reaching a coverage in 2016 that remain almost unchanged in 2018 (see images in Figure 11).

Vegetation encroachment onto river bars initiates pioneer morpholgoical

features that can evolve in mature morphological structures, e.g. islands, stable banks or floodplain. Whether vegetation succeeds in colonising the exposed sediment and grow or it is uprooted before increasing sediment cohesion depends on both river flow and morphology. Therefore, depending on the development stage of vegetation growing on river banks or bars, a flood may be able to remove vegetation and rework the channel bed (e.g. channel widening), or depositing fine sediments promoting vertical accretion of bar or bank advance (i.e channel narrowing). According to this concept the evolutionary trajectory of a river is seen as a sequence of stable and unstable phases resulting from the mutual influence between water flow, vegetation and sediments. The switch between one phase to another is controlled by the water flow and its effect is moderated by the vegetation which is able to engineer the river channel. Therefore, a river system remains in a stable phase until a flood competent for reworking the channel bed occurs, leading to an unstable condition and, at the same time, starting a new cycle (i.e colonised exposed sediments) that will generate a new stable phase (Corenblit et al., 2014).

The simple model proposed provides satisfactory results when applied to the three real cases, with more accurate results for the real channels rather than the laboratory one. In particular, when compared with the laboratory observations the model overestimated the variation in channel width but was capable to correctly predict the overall evolutionary trajectory observed in the flume, with a Pearson correlation coefficient between observed and modelled data equals to 0.69. Results from the application to real scale reaches showed better agreement between the values predicted by the model

and those extracted from the field with a Pearson correlation coefficient estimated of around 0.53 and 0.84 for the case of the LunterseBeek stream and the Thur River respectively. Despite the low correlation value shows by the LunterseBeek case, Figure 10b shows the capability of the model to correctly interpret the evolution and the magnitude of the changes, both for channel width and vegetation biomass, as it was observed in the months following the restoration project of the stream. The comparison between modelled and observed channel width for the three study cases is reported in Figure 12.

The analysis conducted for the case of the river system subject to a stochastic hydrological forcing helps us to interpret how changes in vegetation characteristics, or river hydrology, may affect the overall channel width for the three study cases presented above. In particular, results reported in Figure 8 show that the colonisation process does not affect river channel width, while the increased resistance to sediment erosion provided by plant roots, i.e. high σ_1, significantly narrows the channel cross-section. On the other hand, the colonisation rate, r_1, was found to control the vegetation biomass, with higher values of r_1 determining lower values of vegetation biomass for the effect of increased erosional power due to a narrower channel cross-section. Finally, an increase in flood frequency, λ, promotes the formation of larger channels by augmenting the intensity of the near-bank erosion processes.

It is therefore evident that application of the model requires a preliminary calibration of the parameters against observed data. This is due to a lack of physical relationships describing the interaction between sediment processes and vegetation biomass in the literature. The development of physical relationships linking vegetation biomass to sediment dynamics would allow the

parameter of the model to be estimated on the base of measurable property of the river system, and the model to be universally applied. This problem affects also spatially distributed models for river morphodynamics. On one hand, such models show the advantage of being able to provide a more detailed description of the flow field and sediment dynamics, including bar deposits, thanks to a stronger physical basis for sediment processes. On the other hand, by adopting relationships for vegetation dynamics similar to those we adopted in our model, they still require a preliminary calibration of the parameters when investigating bio-morphological processes (e.g. Bertoldi et al. 2014; Oorschot et al., 2016; Zen et al., 2017; Caponi and Siviglia, 2018). In addition, this type of model requires considerable computational and time efforts to obtain the final result.

Model results have provided evidence that the model developed is able to capture the essential behaviour of the system and could be used, once calibrated against real observations, to predict long term river evolution with extremely low computational effort. The lump model could be used to inform a spatially distributed model for river morphodynamics, such that results from the former would help choosing the input parameters for the latter by pre-selecting river future evolutionary trajectories.

5. Conclusions

We proposed a simple bio-morphodynamic model to investigate the temporal scales of channel width variation and how these relate with that of the hydrologic forcing.

The model is in the form of a dynamical system of two non-linear ordinary

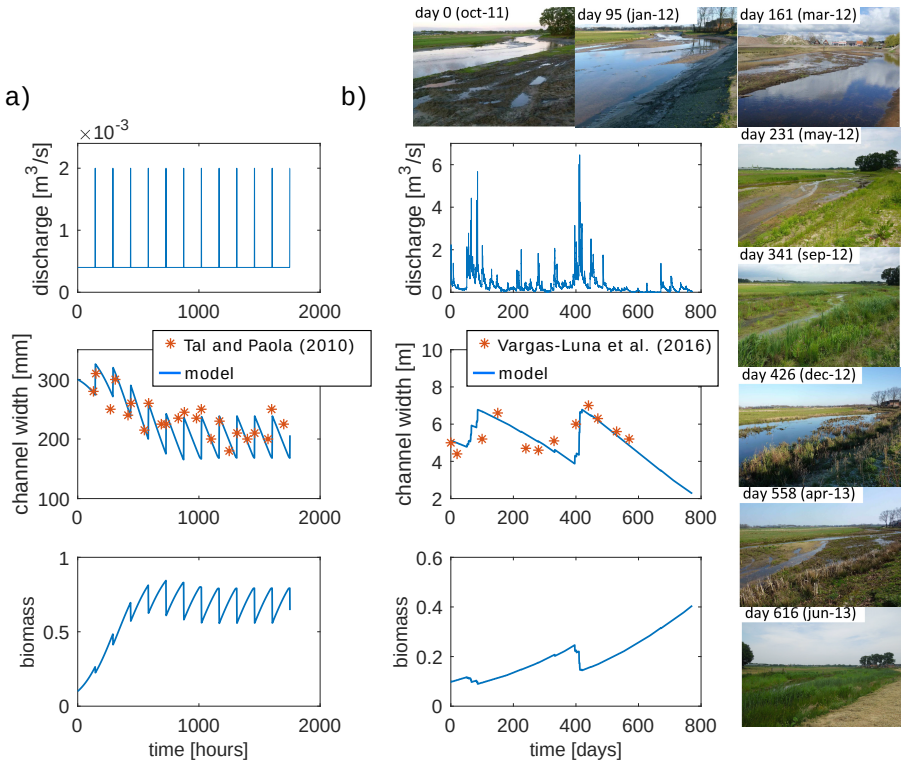

Figure 10: Results from model application to the study case of a) the laboratory run A of Tal and Paola (2010) and b) the Lunterse Beek (Eekhout et al., 2014). The channel width measurements associated to this latter case refer to Vargas-Luna et al. (2016) while the hydrograph can be found at https://www.joriseekhout.com/publications/.

	Q_0^*	w_0^*	S	d_s^*	t_v^*	E^*	r_1	σ_1
	$[m^3/s]$	$[m]$	$[m/m]$	$[m]$	$[years]$	$[m/s]$	$[-]$	$[-]$
Lab flume	$4 \cdot 10^{-4}$	0.3	0.015	$0.5 \cdot 10^{-3}$	2	$9.5 \cdot 10^{-7}$	0.45	0.5
Lunterse Beek	1.4	5	$0.96 \cdot 10^{-3}$	$2.58 \cdot 10^{-4}$	4	$1.58 \cdot 10^{-5}$	3	0.3
River Thur	200	55	10^{-3}	0.02	5	$7.3 \cdot 10^{-3}$	1.5	0.04

Table 1: Model input and coefficients for the application to the flume from the experimental run of Tal and Paola (2010), the Lunterse Beek (Eekhout et al., 2014), and the River Thur (Pasquale and Perona, 2014; Schirmer et al., 2014).

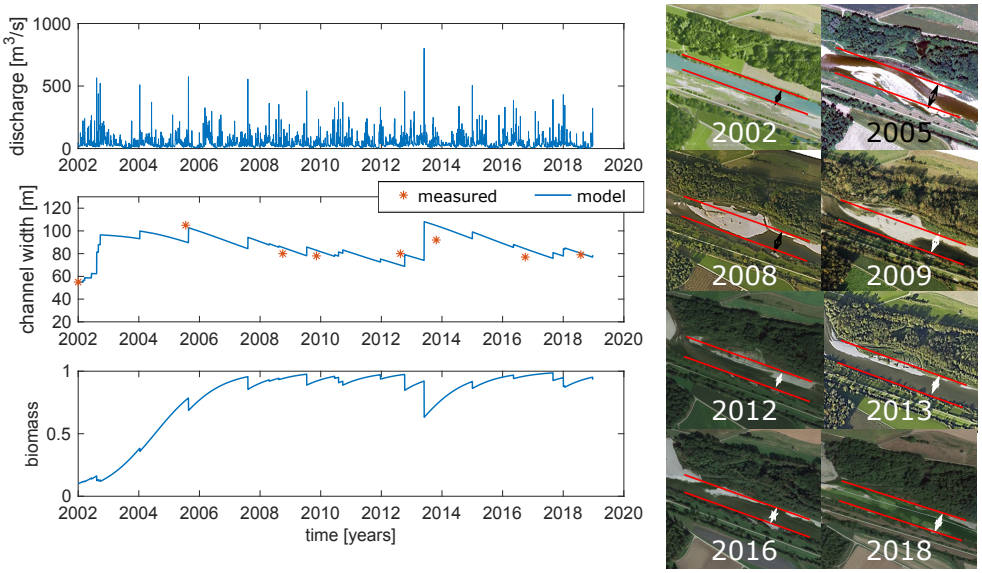

Figure 11: Results from model application to the study case of the Thur River. The exact dates the pictures were taken are: 30/09/2008, 10/11/2009, 19/08/2012, 24/10/2013,30/09/2016/31/07/2018. The date associated to the pictures from 2002 and 2005 is not known. The estimated channel width, in chronological order, is: 55 m, 105 m, 80 m, 78 m, 80 m, 92 m, 77 m, 80 m. Sources Google Earth.

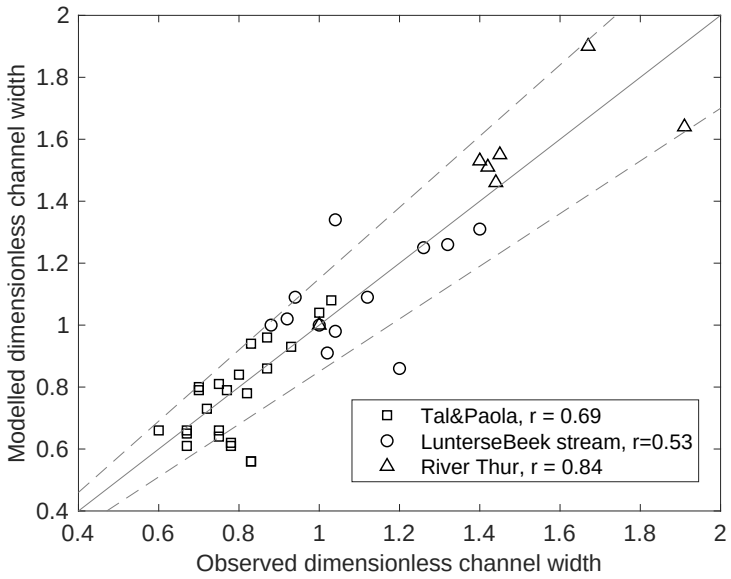

Figure 12: Comparison between observed and modelled channel width for the three study cases: the experimental run of Tal and Paola (2010), the Lunterse Beek (Eekhout et al., 2014), and the River Thur (Pasquale and Perona, 2014; Schirmer et al., 2014). The values are reported in dimensionless form, r is the Pearson correlation coefficient, the solid line is the line of equality, and the dashed lines represent the borders of the 15% confidence interval.

887 differential equations to mimic the interaction between riparian vegetation
888 dynamics and river flow in controlling river channel width temporal adjust-
889 ments. Two distinct mechanisms are considered for channel narrowing and
890 widening occurring at different time scales: the channel narrows because of
891 the vegetation encroachment onto the river bar and widens when the shear
892 stress allows the river bank to be eroded. Different from previous model
893 adopting simplify closure to describe the stabilizing action of the vegetation
894 on the bank (Eke et al., 2014; Lopez Dubon and Lanzoni, 2018; Monegaglia
895 et al., 2019) in this work channel narrowing is directly associated to vegeta-
896 tion dynamics. Furthermore, to fully couple bank and vegetation dynamics
897 vegetation decays during the erosion of the bank and a linear relationship
898 links increases in the critical Shields number for sediment movement with
899 the vegetation biomass.

900 The obtained results have highlighted the limit of adopting simplified
901 discharges in morphodynamic models or regime models to interpret realistic
902 response of the channel. We argued that the use of a constant discharge
903 in morphodynamic models that neglect the root-induced sediment cohesion
904 may overestimate the channel width when compared with real channel cross
905 sections. In addition, the system forced with a high-frequency periodic dis-
906 charge reduced both channel width and vegetation biomass, while increase
907 in flood frequency should generate wider cross sections.

908 The variable-discharge simulations verify that a vegetated channel does
909 not reach a final equilibrium but, because of the cyclical repeat of channel
910 widening and narrowing, keeps oscillating around an asymptotic value as
911 forced by the water flow. Furthermore, these simulations revealed the exis-

tence of an intermediate frequency of floods occurrence for which stochastic bank erosion and deterministic vegetation growth interact leading to a coherent response of the system in time.

The satisfactory results obtained from model application have revealed the potential of the model to be used to interpret the evolutionary trajectories of a channel, once the model parameters have been opportunely calibrated. Because of the high uncertainty affecting the choice of the parameters associated to vegetation dynamics, we have explored how model results are affected by changes in the parameters r_1 and σ_1 accounting, respectively, for the colonisation process and roots action on sediment erosion. We argued how such a problem also affects spatially distributed models for river morphodynamics, which able to provide a more detailed description of in-channel flow field, when investigating bio-morpholgoical interactions.

The present work takes advantage of the minimalist approach and the dimensionless form of the system to explore the interaction between vegetation, water flow and river morphology time scales, by using a low computational effort. The analysis is a first step to include a stochastic dynamic paradigm in a bio-morphodynamic model for river evolution whereby bank properties are directly related to vegetation dynamics which in turn are controlled by both channel morphology and water flow. At the state of the art, model results could inform physically based bio-morphodynamic models for river evolution to optimize the modelling resources. However, in order to obtain quantitative tools that can also support river mangers decisions, research effort is required to quantify the increased resistance to sediment erosion induced by the plant root system. This will also allow model parameters to be

estimated on based on measurable properties of the system rather than to be calibrated.

The model can be included in morphodynamic models for meandering rivers evolution to overcome the limit posed by the simplified closure describing bank deposition and further extend the results obtained by Zen et al. (2016) and Davidson and Eaton (2018). The updated model could be used to investigate the temporal scales of lateral migrating meander bends and relate them to the hydrologic forcing and spatial scales of scroll bars formation in meandering rivers floodplain (Zen et al., 2017; Strick et al., 2018).

Acknowledgments

The authors thank the three anonymous reviewers for their comments that contributed to improve the quality of the paper.

Appendix A: the linear system

The linearized version of the system (18) obtained after expanding in series the three unknown of the problem, $w, \rho, \widetilde{\tau}_{\Delta}$, around their equilibrium values $w_{eq}, \rho_{eq}, \tau_{\Delta,eq}$ reads:

$$\begin{aligned} a_{11}w_1(t) + a_{12}\rho_1(t) + a_{13}\widetilde{\tau}_{\Delta,1}(t) + \frac{dw(t)}{dt} &= 0 \\ a_{21}w_1(t) + a_{22}\rho_1(t) + a_{23}\widetilde{\tau}_{\Delta,1}(t) + \frac{d\rho(t)}{dt} &= 0 \\ a_{31}w_1(t) + a_{32}\rho_1(t) + a_{33}\widetilde{\tau}_{\Delta,1}(t) + \frac{d\widetilde{\tau}_{\Delta}(t)}{dt} &= 0, \end{aligned} \tag{A.1}$$

where the coefficients a_{ij} with i,j = 1,2,3 are:

$$
\begin{aligned}
&a_{11} = \gamma\rho_0; \qquad a_{12} = w_0\gamma; \qquad a_{13} = -E;\\
&a_{21} = -\frac{E\rho_0\widetilde{\tau}_{\Delta,eq}}{w_0^2}; \qquad a_{22} = -1 + 2\rho_0 + \frac{E\widetilde{\tau}_{\Delta,0}}{w_0}; \qquad a_{23} = \frac{E\rho_0}{w_0};\\
&a_{31} = \frac{2t_\Delta\left(\frac{Q}{w_0}\right)^{2/3}\tau_{s,0}\widetilde{\tau}_{\Delta,0}}{3w_0}; \qquad a_{32} = t_\Delta\tau_{c,0}\widetilde{\tau}_{\Delta,0};\\
&a_{33} = t_\Delta\left[\tau_{c,0}(1+\rho_0) - \left(\frac{Q}{w_0}\right)^{(2/3)}\tau_{s,0} + 2\widetilde{\tau}_{\Delta,0}\right];
\end{aligned}
\tag{A.2}
$$

having denoted with $\{w_0, \rho_0, \tau_{\Delta,0}\}$ a stable condition of the system, e.g. the initial bankfull condition.

References

Abramowitz, M., Stegun, I.A., 1965. Handbook of mathematical functions: with formulas, graphs, and mathematical tables. volume 55. Courier Corporation.

Allmendinger, N.E., Pizzuto, J.E., Potter Jr, N., Johnson, T.E., Hession, W.C., 2005. The influence of riparian vegetation on stream width, eastern pennsylvania, usa. Geological Society of America Bulletin 117, 229–243.

Bertagni, M.B., Perona, P., Camporeale, C., 2018. Parametric transitions between bare and vegetated states in water-driven patterns. Proceedings of the National Academy of Sciences 115, 8125–8130.

Bertoldi, W., Siviglia, A., Tettamanti, S., Toffolon, M., Vetsch, D., Francalanci, S., 2014. Modeling vegetation controls on fluvial morphological trajectories. Geophysical Research Letters 41, 7167–7175.

969 Bogoni, M., Putti, M., Lanzoni, S., 2017. Modeling meander morphodynam-
970 ics over self-formed heterogeneous floodplains. Water Resources Research
971 53, 5137–5157.

972 Bolla Pittaluga, M., Luchi, R., Seminara, G., 2014. On the equilibrium
973 profile of river beds. Journal of Geophysical Research: Earth Surface 119,
974 317–332.

975 Botter, G., Porporato, A., Rodriguez-Iturbe, I., Rinaldo, A., 2007. Basin-
976 scale soil moisture dynamics and the probabilistic characterization of car-
977 rier hydrologic flows: Slow, leaching-prone components of the hydrologic
978 response. Water resources research 43.

979 Braudrick, C.A., Dietrich, W.E., Leverich, G.T., Sklar, L.S., 2009. Exper-
980 imental evidence for the conditions necessary to sustain meandering in
981 coarse-bedded rivers. Proceedings of the National Academy of Sciences
982 106, 16936–16941. 10.1073/pnas.0909417106.

983 Camporeale, C., Perucca, E., Ridolfi, L., Gurnell, A., 2013. Modeling the
984 interactions between river morphodynamics and riparian vegetation. Re-
985 views of Geophysics 51, 379–414.

986 Camporeale, C., Ridolfi, L., 2006. Riparian vegetation distribution induced
987 by river flow variability: A stochastic approach. Water Resour. Res. 42.
988 Doi: 10.1029/2006WR004933.

989 Cantelli, A., Wong, M., Parker, G., Paola, C., 2007. Numerical model linking
990 bed and bank evolution of incisional channel created by dam removal.
991 Water Resources Research 43.

992 Caponi, F., Siviglia, A., 2018. Numerical modeling of plant root controls
993 on gravel bed river morphodynamics. Geophysical Research Letters 45,
994 9013–9023.

995 Corenblit, D., Steiger, J., González, E., Gurnell, A.M., Charrier, G., Dar-
996 rozes, J., Dousseau, J., Julien, F., Lambs, L., Larrue, S., et al., 2014.
997 The biogeomorphological life cycle of poplars during the fluvial biogeomor-
998 phological succession: a special focus on populus nigra l. Earth Surface
999 Processes and Landforms 39, 546–563.

1000 Crosato, A., Saleh, M.S., 2011. Numerical study on the effects of floodplain
1001 vegetation on river planform style. Earth Surface Processes and Landforms
1002 36, 711–720.

1003 Darby, S.E., Rinaldi, M., Dapporto, S., 2007. Coupled simulations of fluvial
1004 erosion and mass wasting for cohesive river banks. Journal of Geophysical
1005 Research: Earth Surface 112.

1006 Davidson, S., Eaton, B.C., 2018. Beyond regime: A stochastic model of
1007 floods, bank erosion, and channel migration. Water Resources Research
1008 54. Doi.org/10.1029/2017WR022059.

1009 van Dijk, W.M., van de Lageweg, W.I., Kleinhans, M.G., 2013. Formation of
1010 a cohesive floodplain in a dynamic experimental meandering river. Earth
1011 Surface Processes and Landforms 38, 1550–1565.

1012 Doulatyari, B., Basso, S., Schirmer, M., Botter, G., 2014. River flow regimes
1013 and vegetation dynamics along a river transect. Advances in water re-
1014 sources 73, 30–43.

1015 Eaton, B., Millar, R.G., Davidson, S., 2010. Channel patterns: Braided,
1016 anabranching, and single-thread. Geomorphology 120, 353–364.

1017 Eekhout, J., Fraaije, R., Hoitink, A., 2014. Morphodynamic regime change
1018 in a reconstructed lowland stream. Earth Surf. Dynam 2, 279–293.

1019 Eke, E., Parker, G., Shimizu, Y., 2014. Numerical modeling of erosional
1020 and depositional bank processes in migrating river bends with self-formed
1021 width: Morphodynamics of bar push and bank pull. Journal of Geophysical
1022 Research: Earth Surface 119, 1455–1483.

1023 Erskine, W., Chalmers, A., Keene, A., Cheetham, M., Bush, R., 2009. Role
1024 of a rheophyte in bench development on a sand-bed river in southeast
1025 australia. Earth Surface Processes and Landforms 34, 941–953.

1026 Erskine, W., Keene, A., Bush, R., Cheetham, M., Chalmers, A., 2012. In-
1027 fluence of riparian vegetation on channel widening and subsequent con-
1028 traction on a sand-bed stream since european settlement: Widden brook,
1029 australia. Geomorphology 147, 102–114.

1030 Friedman, J.M., Osterkamp, W.R., Lewis Jr, W.M., 1996. Channel narrowing
1031 and vegetation development following a great plains flood. Ecology 77,
1032 2167–2181.

1033 Gasser, E., Schwarz, M., Simon, A., Perona, P., Phillips, C., Hübl, J., Dorren,
1034 L., 2019. A review of modeling the effects of vegetation on large wood
1035 recruitment processes in mountain catchments. Earth-Science Reviews .

1036 Gurnell, A., 2014. Plants as river system engineers. Earth Surface Processes
1037 and Landforms 39, 4–25.

1038 Gurnell, A., Petts, G., 2006. Trees as riparian engineers: the tagliamento
1039 river, italy. Earth Surface Processes and Landforms: The Journal of the
1040 British Geomorphological Research Group 31, 1558–1574.

1041 Gurnell, A.M., Petts, G.E., Hannah, D.M., Smith, B.P., Edwards, P.J., Koll-
1042 mann, J., Ward, J.V., Tockner, K., 2001. Riparian vegetation and island
1043 formation along the gravel-bed fiume tagliamento, italy. Earth Surface
1044 Processes and Landforms: The Journal of the British Geomorphological
1045 Research Group 26, 31–62.

1046 Howard, A., 1992. Lowland floodplain rivers: Geomorphological perspectives
1047 (ed. by pa carling and ge petts), 1–41.

1048 Howard, A.D., 1980. Thresholds in river regimes. Thresholds in geomorphol-
1049 ogy 227, 227–258.

1050 Ielpi, A., 2018. Morphodynamics of meandering streams devoid of plant life:
1051 Amargosa river, death valley, california. Bulletin 131, 782–802.

1052 Ikeda, S., Parker, G., Sawai, K., 1981. Bend theory of river meanders. Part
1053 1 - Linear development. J. Fluid Mech. 112, 363–377.

1054 Kaplan, D., Glass, L., 1995. Understanding Nonlinear Dynamics. Springer-
1055 Verlag, Berlin, Heidelberg.

1056 van de Lageweg, W.I., van Dijk, W.M., Baar, A.W., Rutten, J., Kleinhans,
1057 M.G., 2014. Bank pull or bar push: What drives scroll-bar formation in
1058 meandering rivers? Geology 42, 319–322.

1059 Langendoen, E.J., Richard Lowrance, R., Simon, A., 2009. Assessing the im-
1060 pact of riparian processes on streambank stability. Ecohydrology: Ecosys-
1061 tems, Land and Water Process Interactions, Ecohydrogeomorphology 2,
1062 360–369.

1063 Lanzoni, S., Luchi, R., Pittaluga, M.B., 2015. Modeling the morphodynamic
1064 equilibrium of an intermediate reach of the po river (italy). Advances in
1065 water resources 81, 95–102.

1066 Lanzoni, S., Seminara, G., 2006. On the nature of meander instability. Jour-
1067 nal of Geophysical Research: Earth Surface 111.

1068 Lopez Dubon, S., Lanzoni, S., 2018. Meandering evolution and width vari-
1069 ations: a physics-statistics based modeling approach. Water Resources
1070 Research Doi.org/10.1029/2018WR023639.

1071 Matsubara, Y., Howard, A.D., Burr, D.M., Williams, R.M., Dietrich, W.E.,
1072 Moore, J.M., 2015. River meandering on earth and mars: A comparative
1073 study of aeolis dorsa meanders, mars and possible terrestrial analogs of the
1074 usuktuk river, ak, and the quinn river, nv. Geomorphology 240, 102–120.

1075 Micheli, E., Kirchner, J., 2002. Effects of wet meadow riparian vegetation
1076 on streambank erosion. 1. remote sensing measurements of streambank
1077 migration and erodibility. Earth Surface Processes and Landforms 27,
1078 627–639.

1079 Micheli, E., Kirchner, J., Larsen, E., 2004. Quantifying the effect of ripar-
1080 ian forest versus agricultural vegetation on river meander migration rates,

central sacramento river, california, usa. River research and applications 20, 537–548.

Millar, R.G., 2000. Influence of bank vegetation on alluvial channel patterns. Water Resources Research 36, 1109–1118.

Monegaglia, F., Tubino, M., Zolezzi, G., 2019. Interaction between curvature-driven width oscillations and channel curvature in evolving meander bends. Journal of Fluid Mechanics 876, 985–1017.

Murray, A.B., Paola, C., 2003. Modelling the effect of vegetation on channel pattern in bedload rivers. Earth Surface Processes and Landforms: The Journal of the British Geomorphological Research Group 28, 131–143.

Nanson, G.C., 1981. New evidence of scroll-bar formation on the beatton river. Sedimentology 28, 889–891.

Oorschot, M.v., Kleinhans, M., Geerling, G., Middelkoop, H., 2016. Distinct patterns of interaction between vegetation and morphodynamics. Earth Surface Processes and Landforms 41, 791–808.

Parker, G., 1998. River meanders in a tray. Nature 395, 111.

Parker, G., Paola, C., Whipple, K.X., Mohrig, D., 1998. Alluvial fans formed by channelized fluvial and sheet flow. i: Theory. Journal of Hydraulic Engineering 124, 985–995.

Parker, G., Shimizu, Y., Eke, G.W.E., Abad, J., Lauer, J., Paola, C., Dietrich, W., Voller, V., 2011. A new framework for modeling the migration

of meandering rivers. Earth Surface Processes and Landforms 36, 70–86. Doi:10.1002/esp.2113.

Pasquale, N., Perona, P., 2014. Experimental assessment of riverbed sediment reinforcement by vegetation roots. River Flow , 553–561.

Perona, P., Molnar, P., Crouzy, B., Perucca, E., Jiang, Z., McLelland, S., Wüthrich, D., Edmaier, K., Francis, R., Camporeale, C., et al., 2012. Biomass selection by floods and related timescales: Part 1. experimental observations. Advances in Water Resources 39, 85–96.

Perucca, E., Camporeale, C., Ridolfi, L., 2007. Significance of the riparian vegetation dynamics on meandering river morphodynamics. Water Resources Research 43.

Pizzuto, J., O'Neal, M., Stotts, S., 2010. On the retreat of forested, cohesive riverbanks. Geomorphology 116, 341–352.

Pizzuto, J.E., 1984. Bank erodibility of shallow sandbed streams. Earth surface processes and landforms 9, 113–124.

Pizzuto, J.E., 1994. Channel adjustments to changing discharges, powder river, montana. Geological Society of America Bulletin 106, 1494–1501.

Pollen, N., Simon, A., 2005. Estimating the mechanical effects of riparian vegetation on stream bank stability using a fiber bundle model. Water Resources Research 41.

Ridolfi, L., D'Odorico, P., Laio, F., 2011. Noise-induced phenomena in the environmental sciences. Cambridge University Press.

1124 Rinaldi, M., Mengoni, B., Luppi, L., Darby, S.E., Mosselman, E., 2008.
1125 Numerical simulation of hydrodynamics and bank erosion in a river bend.
1126 Water Resources Research 44.

1127 Santos, M.G., Hartley, A.J., Mountney, N.P., Peakall, J., Owen, A., Merino,
1128 E.R., Assine, M.L., 2019. Meandering rivers in modern desert basins:
1129 Implications for channel planform controls and prevegetation rivers. Sedi-
1130 mentary Geology 385, 1–14.

1131 Schirmer, M., Luster, J., Linde, N., Perona, P., Mitchell, E.A., Barry, D.A.,
1132 Hollender, J., Cirpka, O.A., Schneider, P., Vogt, T., et al., 2014. Morpho-
1133 logical, hydrological, biogeochemical and ecological changes and challenges
1134 in river restoration–the thur river case study. Hydrology and Earth System
1135 Sciences 18, 2449–2462.

1136 Seminara, G., 2006. Meanders. Paper invited for the 50th Anniversary issue
1137 of the J. Fluid. Mech. 554, 271–297. DOI: 10.1017/S0022112006008925.

1138 Strick, R.J., Ashworth, P.J., Awcock, G., Lewin, J., 2018. Morphology and
1139 spacing of river meander scrolls. Geomorphology 310, 57–68.

1140 Strogatz, S.H., 2018. Nonlinear dynamics and chaos: with applications to
1141 physics, biology, chemistry, and engineering. CRC Press.

1142 Tal, M., Paola, C., 2010. Effects of vegetation on channel morphodynam-
1143 ics: results and insights from laboratory experiments. arth Surf. Process.
1144 Landforms 35, 1014–1028.

1145 Tealdi, S., Camporeale, C., Ridolfi, L., 2011. Long-term morphological river

response to hydrological changes. Advances in water resources 34, 1643–1655.

Thorne, C.R., 1990. Effects of vegetation on riverbank erosion and stability. Wiley. British Geomorphological Research Group Symposia Series. URL: https://books.google.co.uk/books?id=7rsPAQAAIAAJ.

Thorne, C.R., 1998. River width adjustment. i: Processes and mechanisms. J. Hydraul. Eng 124, 881–902.

Tubino, M., 1991. Growth of alternate bars in unsteady flow. Water Resources Research 27, 37–52.

Van Dijk, W., Teske, R., Van de Lageweg, W., Kleinhans, M., 2013. Effects of vegetation distribution on experimental river channel dynamics. Water Resources Research 49, 7558–7574.

Vargas-Luna, A., Crosato, A., Hoitink, A., Groot, J., Uijttewaal, W., 2016. Effects of riparian vegetation development in a restored lowland stream, in: River Flow.

Vesipa, R., Camporeale, C., Ridolfi, L., 2017. Effect of river flow fluctuations on riparian vegetation dynamics: Processes and models. Advances in Water Resources 110, 29–50.

Wiel, M.J.V.D., Darby, S.E., 2007. A new model to analyse the impact of woody riparian vegetation on the geotechnical stability of riverbanks. Earth Surface Processes and Landforms: The Journal of the British Geomorphological Research Group 32, 2185–2198.

1168 Yang, S., Bai, Y., Xu, H., 2018. Experimental analysis of river evolution
1169 with riparian vegetation. Water 10, 1500. Doi:10.3390/w10111500.

1170 Zen, S., Gurnell, A.M., Zolezzi, G., Surian, N., 2017. Exploring the role of
1171 trees in the evolution of meander bends: The t agliamento r iver, i taly.
1172 Water Resources Research 53, 5943–5962.

1173 Zen, S., Zolezzi, G., Toffolon, M., Gurnell, A.M., 2016. Biomorphodynamic
1174 modelling of inner bank advance in migrating meander bends. Advances
1175 in water resources 93, 166–181.

1176 Zen, S., Zolezzi, G., Tubino, M., 2014. A theoretical analysis of river bars
1177 stability under changing channel width. Advances in Geosciences 39, 27–
1178 35.